The Transient Response of the North Atlantic: Some Model Studies

DAVID L. T. ANDERSON[1] KIRK BRYAN A. E. GILL[1] AND R. C. PACANOWSKI

Geophysical Fluid Dynamics Laboratory, Princeton University, Princeton, New Jersey 08540

Four numerical experiments have been designed to clarify the role of stratification and topography on the transient response of the ocean to a change in wind forcing. The geometry and topography appropriate to the North Atlantic between the equator and 50°N are used to make the study more appropriate to a real ocean. In all four experiments, zonally symmetric wind stresses are 'switched on' at the upper surface of a resting model ocean. Two short experiments, 1 and 2, with a duration of 100 days, are first discussed. These are for a homogeneous ocean with and without topography. The response in the flat-bottomed case can be described either in terms of planetary waves or basin modes, but when topography is present, no obvious wave propagation was identified. Higher-frequency basin modes are detectable, but their amplitude is much lower than that in the flat-bottomed case. They are damped out on a time scale of ~50 days. Two longer experiments, 3 and 4, are then analyzed. These are the analogs of 1 and 2, but stratification was included. The introduction of stratification for the ocean with topography leads to a new, longer time scale, not just for the baroclinic modes, but also for the barotropic. Despite the presence of topography, modal analysis was found useful in analyzing the results. Propagation effects are analyzed, both on the moderately fast time scale of internal Kelvin waves and on the slow time scale of internal planetary waves. Kelvin waves are apparent along the equator, the northern boundary, and on the eastern coast in the Gulf of Guinea from the equator to 20°N. They are not clearly visible anywhere on the west coast. Planetary waves can be detected in the interior both in the presence and absence of topography. When topography is present without stratification, the transport of the Gulf Stream is reduced from 30 to 14 million tons per second. This is a well-known result. With stratification there is no significant difference in transport between the case with or without topography.

1. Introduction

In this paper we will present the results of a series of numerical experiments designed to clarify aspects of the circulation of the Atlantic Ocean. We will concentrate on the transient response, and it will be found that planetary waves and basin modes will be useful tools in understanding the circulation. The role of planetary waves in the temporal response of the ocean has been examined by several authors. *Pedlosky* [1965*a*, *b*], *Phillips* [1966], *Veronis* [1963, 1966, 1970], and *Veronis and Stommel* [1956] have considered time-dependent wind forcing, *Gates* [1968] has examined the barotropic spin-up of a mid-latitude ocean, and *Lighthill* [1969] has considered aspects of the low-latitude response. *Anderson and Gill* [1975] unified various parts of the mid-latitude spin-up problem for the case of east-west forcing which is periodic in the north-south direction for an ocean with north-south coasts. The dynamical equatorial response has been considered by *Yoshida* [1959], *Blandford* [1966], *Matsuno* [1966], *Moore* [1968], *Lighthill* [1969], *Gill* [1975], *Hurlburt et al.* [1976], *Anderson and Rowlands* [1976], and *Cane and Sarachik* [1976]. *Longuet-Higgins* [1964, 1965*a*, *b*] has contributed substantially to both the planetary wave and the basin mode picture.

The above analyses, however, have tended to look at specific aspects, usually in idealized ocean basins and with simple wind patterns. Here we consider the case of more realistic wind forcing and also use a geometry and topography similar to that of the North Atlantic. The latitudinal extent of the model is from 50°N to the equator, where reflectional symmetry is implied. Thus we should be able to consider both equatorial and middle latitude response and the effects of geometry and topography.

The wind stress used is uniform in the x direction, steady in time, and has a latitudinal distribution given by

$$X = 0.2 - 0.8 \sin(2\pi\phi/57.3) - 0.5[1 - \tanh(10.05\phi/57.3)] \quad (1)$$

where ϕ is in the range $-0.5°$ to $50.5°$. This is plotted as a function of latitude in Figure 1.

Four experiments will be analyzed. The first two are spin-up calculations for a homogeneous ocean. Since the barotropic response is fairly rapid, the main dynamic adjustment takes place within days. However, there are transient effects which are felt for much longer, so the calculations were run for 100 days. The first experiment (experiment 1) had no topography, while the second (experiment 2) had that appropriate to the North Atlantic. A comparison between 1 and 2 highlights the effects of topography on the transient barotropic response. In 1 there are indications of planetary wave trains. There are no such indications in 2, though basin modes of reduced amplitude are present. Two further experiments were carried out: the stratified versions of 1 and 2, labeled 3 and 4, respectively. The introduction of stratification allows a much slower baroclinic response, and to get some measure of this, experiments 3 and 4 were run for 1600 days. The experiments are summarized in Table 1. In experiments 3 and 4 the stratification is assumed uniform in (x, y) and varies only in the vertical. There are no mean currents, and in all cases the dynamics is linear to allow a closer comparison with the substantial body of linear theory.

In section 3, results from a flat homogeneous calculation will be compared with wave theory and with results from a homogeneous calculation with realistic bottom topography. The effect of topography on basin modes will prove important for an understanding of the differences between the two calculations, the presence of higher frequencies, and the lack of coherence in the topographic case. Then in section 4, stratification is added, the rapid internal response in low latitudes and along boundaries being considered first. In section 5, results from much longer calculations are presented.

Many of the analytical tools needed for analysis of the results are brought together in section 2. The experienced

[1] Now at Department of Applied Mathematics and Theoretical Physics, Cambridge University, Cambridge, England.

Paper number 8C0776.
0148-0227/79/008C-0776$01.00

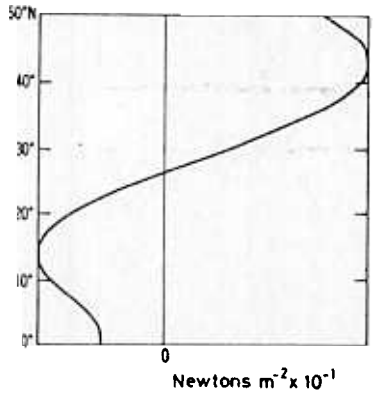

Fig. 1. Plot of the westward wind stress as a function of latitude used in the model (experiment 1). This has extrema at 14°N and 43°N, a zero crossing at 27°N, and zero curvature at 8°N and 29°N.

reader may wish to pass right over this section to the following sections. A brief description of the numerical model is given in Appendix A. The purpose of this work is to unify the various approaches that have been hitherto developed with a view to determining the importance of effects that have made analysis difficult, such as geometry and topography. This study is a detailed examination of how a realistic ocean basin could be expected to spin up. However, this is only the first stage in understanding the more complicated observed response. This study in itself will not provide a total understanding of the ocean behavior. Further work is needed to increase the realism of the simulation. For example, a study of the response of currents to the seasonal variation of wind is in progress.

2. Review of Relevant Theory

In this section we will give a brief review of many of the results of middle latitude and equatorial wave dynamics that we will require and set down the formalism for the analysis used in later sections. We begin by discussing vertical modes.

a. *Modal Analysis*

The model has 12 vertical levels, distributed so as to resolve properly the thermocline and the surface layers. The actual depths are given in Table A1. It will prove useful in analyzing results to split the vertical response into a barotropic component and 11 baroclinic components. The former represents the total integrated transport, and the baroclinic modes, for which the integrated transport is zero, represent perturbations to the temperature field. Following *Gill and Clarke* [1974], we will define a mode to be the eigensolution of

$$w_{nzz} + \frac{N^2}{c_n^2} w_n = 0 \tag{2}$$

with $w_n = 0$ at $z = 0, -H$ and where c_n, the mode speed, is the eigenvalue and N is the Brunt-Väisälä frequency. Then each mode satisfies the equations

TABLE Description of Experiments

Experiment	Type	Topography	Duration, days
1	homogeneous	no	100
2	homogeneous	yes	100
3	stratified	no	1600
4	stratified	yes	1600

$$u_t^n - fv^n = -p_x^n + X \tag{3}$$

$$v_t^n + fu^n = -p_y^n \tag{4}$$

$$p_t^n + c_n^2(u_x^n + v_y^n) = 0 \tag{5}$$

where $u = \sum_{n=0}^{M-1} u^n W_{nz}(z)$, $p = \sum_{n=0}^{M-1} p^n W_{nz}(z)$, $X = \sum_{n=0}^{M-1} X^n W_{nz}(z)$, X is the body force, representing the wind stress in the x direction distributed as a body force over some depth H_{mix}, and M is the number of levels in the vertical (which may be infinite but for this study is 12).

As was pointed out by *Moore and Philander* [1977], the relative distribution of the model amplitudes of the forcing depends critically on the depth of this layer H_{mix}. In particular,

$$\sum_{n=1}^{11} \left(\frac{X^n}{X^0}\right)^2 = \frac{H}{H_{mix}} \quad \text{or} \quad \frac{H}{H_{mix}} \tag{6}$$

For H_{mix} = 50, 113, and 204 m, the depths of the top three model levels, this ratio has the value 101, 44, and 24, so a shallower surface mixed layer tends to accentuate the baroclinic modes relative to the barotropic. The fractional variance accounted for by the barotropic mode is precisely H_{mix}/H. It is clear that the shallower the mixed layer, the more the higher modes are excited. *Lighthill* [1969] in his paper on the spin-up of the Somali current uses an H_{mix} of 200 m (though with a different stratification than that used here). Since we are uncertain as to how exactly the effects of the wind are felt by the ocean, there must remain some ambiguity in model results. For the calculations reported here, H_{mix} was 50 m, corresponding to the wind being applied as a body force over the top model level. While qualitatively the behavior of the model response should hold good irrespective of the value of H_{mix} (50, 113, or 204 m, equivalent to applying the wind over the top one, two, or three model levels), the relative amplitudes of the modes would be different, and this could result in different values for the magnitudes of the relative effects.

The spherical polar forms of (2) and (3) are valid over all latitudes, but it is easier to consider approximations to (2) and (3) which are valid either in middle latitudes ($f = f_0 + \beta y$) or in the equatorial zones ($f = \beta y$). We will consider these two regions separately and then consider the transition between the two.

b. *Middle Latitude Response*

Equations (3)–(5) can be recast as [*Anderson and Gill*, 1975]

$$p_{xxt} + p_{yyt} - \frac{f^2}{c^2} pt + \beta p_x = -f^2\left(\frac{X}{f}\right)_y \approx -fX_y \tag{7}$$

$$u_{xxt} + u_{yyt} - \frac{f^2}{c^2} u_t + \beta u_x = X_{yy} \tag{8}$$

$$v_{xxt} + v_{yyt} - \frac{f^2}{c^2} v_t + \beta v_x = \frac{f}{c^2} X_t \tag{9}$$

where certain small terms have been discarded and inertial oscillations have been excluded. In the above, f can be taken as constant. Equations (7)–(9) have several interesting properties.

There is a marked discrepancy between the magnitude of the f^2/c^2 term in the barotropic and baroclinic cases. For the barotropic mode, using the density distribution given in Appendix A, c = 224 m/s, while for the first baroclinic mode, c = 2.71 m/s. Thus f^2/c^2 has the respective values 0.25×10^{-12} and 1.0×10^{-9} m^{-2}. Typically, for periodic forcing of north-south wave number l, the y curvature term has a magnitude l^2 which

is of order 10^{-12} m^{-2}. Thus for the barotropic case this is the dominant term, while for the baroclinic modes the f^2/c^2 term dominates (c/f is often called the radius of deformation and is different for each mode, being typically of the order of 30 km but varying with latitude and mode). There is an interior baroclinic response to (7)–(9):

$$p_t = (c^2/f)X_y t$$
$$u_t = -(c^2/f^2)X_{yy}t \tag{10}$$
$$v_t = -X/f$$

in which the perturbation pressure and zonal velocity increase linearly with time but in which the meridional velocity attains a steady value (inertial oscillations have been excluded). The time for the interior zonal velocity to become comparable with the interior meridional velocity is f/l^2c^2. For the first internal mode this time is ~100 days, longer for the higher internal modes. Plane wave solutions exist to (7)–(9) with dispersion relation [*Longuet-Higgins*, 1964]:

$$\omega = -\frac{\beta k}{(k^2 + l^2 + f^2/c^2)} \tag{11}$$

where k is the east-west wave number. The speed of the fastest planetary waves is $\beta/(l^2 + f^2/c^2)$, which for the barotropic mode is 20 m/s and for the first baroclinic is 1–2 cm/s.

Anderson and Gill [1975] showed how long planetary waves traveling westward from a coast at $x = L$ would slow down the interior buildup in u and leave a steady state Sverdrup flow behind:

$$u = \frac{X_{yy}}{\beta}(x - L) \tag{12}$$

Short planetary traveling eastward from a coast at $x = -L$ can establish a western boundary current

$$u - \frac{c^2 l^2 X}{f^2}\left\{t \quad \left[\frac{t}{\beta(x + L)}\right]^{1/2} J_1[2((L + x)\beta t)^{1/2}]\right\} \tag{13}$$

while the long planetary waves can eventually alter this boundary development to

$$u = \frac{-l^2}{\beta} X\{2LJ_0[2((x + L)\beta t)^{1/2}] - L + x\} \tag{14}$$

provided friction effects have not yet become dominant. A thinning boundary layer of the form (14) has been discussed for barotropic waves in the equatorial region by *Lighthill* [1969]. The intermediate form (13) applies only to the baroclinic case. In the barotropic case the large value for the radius of deformation and the rapid speeds of the long Rossby waves mean that there is little time for the short Rossby waves to establish a western boundary current before the long waves modify it.

At a north-south coast the boundary condition is $u = 0$, which implies

$$\frac{-p_y}{f} - \frac{p_{xt}}{f^2} = 0 \tag{15}$$

On the β plane there is no well-defined x scale, though (7) does have the scale $\pm f/c$, which is obtained by balancing the first and third terms. This scale is appropriate for a time for which β effects are negligible. Then (15) becomes (for trapping at an eastern boundary in the northern hemisphere)

$$p_t + cp_y = 0 \tag{16}$$

This is the equation of a coastal Kelvin wave traveling northward along this boundary. Planetary waves will tend to broaden this upwelling zone, but the time scale of the broadening is longer than that required for the passage of a Kelvin wave, so both effects can coexist.

c. *Equatorial Dynamics*

If the equatorial β plane approximation ($f = \beta y$) is made, the solution to (3)–(5) can be expressed in terms of parabolic cylinder functions. The appropriate scalings are

$$x^* = \frac{x}{a} \qquad y^* = \frac{y}{a} \qquad t^* = \frac{ct}{a}$$
$$u^* = \frac{u}{c} \qquad v^* = \frac{v}{c} \qquad p^* = \frac{p}{c^2} \qquad X^* = \frac{aX}{c^2} \tag{17}$$

where $a = (c/2\beta)^{1/2}$ has been termed by Gill the equatorial radius of deformation. The equations for p, u do not decouple in this case, and thus it is useful to introduce new variables [*Gill and Clarke*, 1974],

$$q^* = p^* + u^*$$
$$r^* = p^* - u^* \tag{18}$$

when q^*, r^*, v^*, X^* are decomposed into parabolic cylinder functions

$$q^*(y) = \sum q^m D_m(y) \tag{19}$$

then (3)–(5) can be written [*Anderson and Rowlands*, 1976]

$$q_t{}^0 + q_x{}^0 = X^0 \tag{20}$$

$$2r_{ttt}{}^m - 2r_{xxt}{}^m + (2m + 3)r_t{}^m - r_x{}^m = -2X_{tt}{}^m + (m + 1)(m + 2)X^{m+2} - (m + 2)X^m \tag{21}$$

$$2q_{ttt}{}^{m+2} - q_{xxt}{}^{m+2} + (2m + 3)q_t{}^{m+2} - q_x{}^{m+2} = 2X_{tt}{}^{m+2} + (m + 1)X^{m+2} - X^m \tag{22}$$

$$2v_{ttt}{}^{m+1} - 2v_{xxt}{}^{m+1} + (2m + 3)v_t{}^{m+1} - v_x{}^{m+1} = -X_t{}^m - (m + 2)X_t{}^{m+2} \quad m = 0, 2, 4, \cdots \tag{23}$$

where only those modes with the correct symmetry with respect to the equator have been retained. (We have imposed reflectional symmetry about the equator.)

The lowest-order wave is the Kelvin wave (20). It is nondispersive and travels eastward at speed unity in nondimensional form or c in dimensional units. The next lowest order is the equation for r^0, which in dimensional form has gravity inertia waves traveling at a maximum speed c, Rossby waves traveling westward at speed $c/3$ and eastward at speed $c/24$, but this latter wave is probably susceptible to dissipation. In general, the long planetary waves travel westward at speed $c/(2m + 3)$, $m = 0, 2, 4, 6, \cdots$. For any given mode we expect to see waves at speed c, $c/3$, $c/7$, $\cdots$, westward and c eastward.

In the interior, in the absence of boundary effects, the frequencies excited are given by ($k = 0$)

$$\omega = [(2m + 3)\beta c]^{1/2} \quad m = 0, 2, 4, \cdots \tag{24}$$

which are gravity inertia waves. The equatorial region thus has a discrete set of frequencies and wave speeds for each mode (in contrast to middle latitudes, where there is only one frequency and one wave speed). The richness of the spectral (and wave response near the equator) will be analyzed in section 4. The dispersion relation corresponding to (21)–(23) is given below

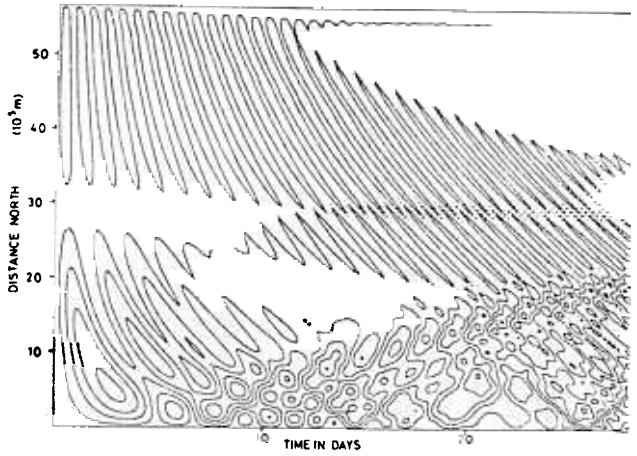

Fig. 2a. Contours of v obtained by integrating (26)–(28). Note the inertial shadow zone poleward of the wave front initiated at the northern boundary and traveling equatorward.

in (25) for comparison with the middle latitude result. This latter cannot be obtained from (9), since gravity inertia waves have been excluded, but an equation for v can be obtained without recourse to filtering. It is the same as (9) but with $-v_{ttt}/c^2$ added to the left-hand side:

$$k^2 + \beta/\omega k + (2m+3)\beta/c - \omega^2/c^2 = 0$$
$$k^2 + \beta/\omega k + (f^2 + f^2/c^2) - \omega^2/c^2 = 0 \qquad (25)$$

High values of m will extend the equatorial solution into higher latitudes.

d. *Transient Response in the Absence of Meridional Boundaries*

As a preliminary to the main study, it is useful to consider how a particular mode responds when no meridional boundaries are present, the wind stress $X(y)$ being applied at some initial instant and then held constant. Solutions to this problem involve only one space dimension (y) and time. Equations (3) to (5) in this case can be rearranged as

$$u_t = +fv + X \qquad (26)$$
$$v_t = -fu - p_y \qquad (27)$$
$$p_t = -c^2 v_y \qquad (28)$$

Solutions to (26)–(28) have been discussed for X uniform by *Moore and Philander* [1977] for a short calculation. *Gill* [1975] has considered the steady solution, i.e., with inertial oscillations suppressed. The solutions with uniform X nicely illustrate the development of the equatorial jet [*Yoshida*, 1959], but the solution with variable X is more appropriate for later comparisons with the model and will be discussed here. The solution for v, p with $X(y)$ given by (1) is shown in Figures 2*a* and 2*b* as a function of y and t. The calculation was made using the equatorial β plane approximations, i.e., putting $f = \beta y$ and replacing ϕ in (1) by y/R, where R is the radius of the earth. A northern boundary was placed at $y = 5.7 \times 10^6$ m, corresponding to the boundary at 50°N in the model experiments.

An equation for v can be obtained from (26)–(28). It is

$$\frac{v_{tt}}{f^2} - \frac{c^2}{f^2} v_{yy} + v = -\frac{X}{f} \qquad (29)$$

We see that if inertial oscillations are excluded, then for motions for which the north-south scale is larger than the radius of deformation c/f, v can be approximated by

$$v = -\frac{X}{f} - \frac{c^2}{f^2}\left(\frac{X}{f}\right)_{yy}$$

implying

$$p_t = c^2\left(\frac{X}{f}\right)_y \qquad (30)$$
$$u_t = \frac{-c^2}{f}\left(\frac{X}{f}\right)_{yy}$$

The first term in the v solution is just the Ekman balance $v = -X/f$. In Figure 2*c* we plot the solutions to (29), excluding inertial oscillations. For comparison, the Ekman solution $-X/f$ is plotted as a dashed curve. It is a very good approximation to quite low latitudes, ~10°N. We now consider the time dependent solution to (29) given for v and p in Figures 2*a* and 2*b*. Initially, v increases quadratically with time and has the form $v = -fXt^2/2$. Transients readjust the profile to $-X/f$ except within the equatorial zone. The transients are particularly noticeable in the equatorial zone, where they are of large amplitude. At higher latitudes there is a lot of high-frequency inertial oscillation as well as propagation. (The frequency at a given value of y increases: inertial oscillations appear at the point where the forcing is zero.) Near the northern boundary

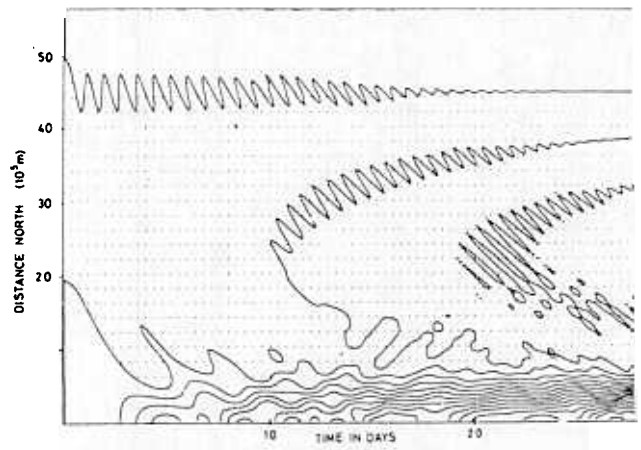

Fig. 2b. Contours of p obtained by integrating (26)–(28)

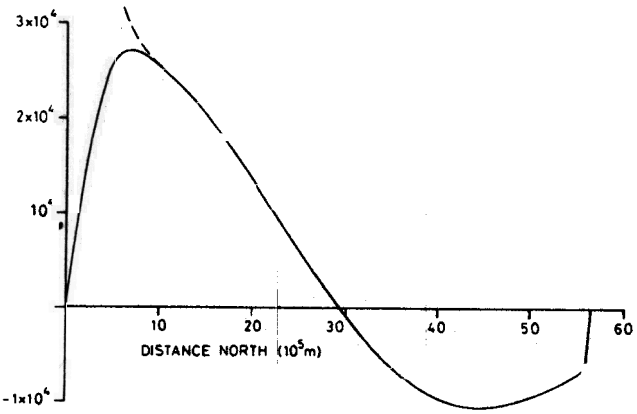

Fig. 2c. Plot of the steady state solution v (solid line) to (29) and of the Ekman solution (dashed line).

an inertial shadow zone appears, which is associated with the ray from the northern boundary. The nature of this shadow zone and the propagation of inertial energy in this dispersive medium have been considered by *Anderson and Gill* [1979].

Figure 2*b* shows the fine northern boundary scale on which p changes and hence on which a zonal boundary current is established. It is the radius of deformation $c/f \sim 20$ km. The linear increase in p along this and the equatorial boundary will not go on indefinitely in a bounded basin because waves from the meridional boundaries (equatorial Kelvin, Rossby, or coastal Kelvin waves) will cancel out this effect.

e. *Effects of Topography in a Homogeneous Ocean*

Steady state solutions to homogeneous oceans with and without topography have been studied extensively (see *Schulman* [1975] for a review). In the linear inviscid case, flow is expected to obey $(D/Dt)(f/H) = 0$, that is, the flow follows contours of f/H.

Westward flow approaching a shallowing bottom is deflected equatorward. Thus the Gulf Stream is likely to be weaker in the topography case. The topography may also be important in determining the point at which the stream separates from the coast.

Time dependent solutions have been examined by *Anderson and Killworth* [1977] for topography varying only in the east-west direction. The analysis, appropriate for middle latitudes, allows an extension of the results of *Longuet-Higgins* [1964] on basin modes and *Anderson and Gill* [1975] on planetary wave behavior. The governing equation is

$$u_{xxt} + u_{yyt} - \frac{f^2}{c^2(1 - T(x)/H)} u_t + \beta u_x - \frac{fT_x}{H(1 - T(x)/H)} u_y = X_{yy} \qquad (31)$$

which should be contrasted with (8). T is the height of the topography measured upward from the reference level $z = -H$ and $c = (gH)^{1/2}$.

Basin modes, that is, solutions of the form $\phi(x) \exp[i(ly + \omega t + \beta x/2\omega)]$, where ϕ is a solution of

$$\phi_{xx} + \phi\left(\beta^2/4\omega^2 - l^2 - \frac{f^2}{c^2(1 - T/H)} - g/\omega\right) = 0 \qquad (32)$$

and $g = +lfT_x/H(1 - T/H)$ with boundary conditions $\phi = 0$ at $X = \pm L$, play an important role in the time response. For zero topography, solutions exist for

$$\omega = \frac{\beta}{2[(n^2\pi^2/4L^2) + l^2 + f^2/c^2]^{1/2}} \qquad n = 1, 2, 3 \qquad (33)$$

which corresponds to a period of 7 days for $L = 3 \times 10^6$ m, $\beta = 2 \times 10^{-11}$ m^{-1} s^{-1}, $l = 10^{-6}$ m^{-1}, $c = 224$ m/s, and $n = 1$. A mid-Atlantic ridge with a height of only 1700 m would, according to *Anderson and Killworth* [1977], reduce the period of the basin mode to approximately 2/5 of the above value.

Actually, (33) implies two values of ω for any order of solution n, but these frequencies ω_+, ω_- are identical in magnitude for the flat-bottomed case. When $g \neq 0$, such a simple expression for the eigenvalues as (33) no longer exists, $|\omega_+|$ is no longer equal to $|\omega_-|$, and the solutions are distinct. The solutions with lowest $|\omega|$ correspond to solutions trapped over the ridge. Further analysis of basin modes in closed geometries has been made by *Platzman* [1975] and *Ripa* [1978], who find qualitatively similar results.

The dynamics of the spin-up of (31) is similar to that given by *Anderson and Gill* [1975] except that the appropriate solution about which there exist wavelike solutions is the topographic Sverdrup solution, that is, solutions of [see *Schulman*, 1975]

$$\beta u_x - \frac{ilfT_x}{(H - T)} u = -l^2 X \qquad (34)$$

The position and amplitude of the topography have a strong effect on the amplitude of u mainly westward of the topography. A thinning boundary layer exists at the western boundary as in the case without topography.

f. *Effects of Topography in a Stratified Ocean for Topography Varying in the East-West Direction*

The interaction of topography and stratification, Jebar [see *Sarkisyan and Keondjiyan*, 1975], is usually between a mean stratification which can vary with (x, y) and topography. In this section and in section 5 the mean stratification is independent of x and y, but a Jebar effect can still take place. In this latter case the variation in stratification is self-induced by the internal waves and thus within the framework of the model consistent with the flow field and the topography. Some of the problems inherent in using an 'observed' density field are thus avoided.

In this section we will review the effect topography has on the propagation of information. The stratification is taken independent of x, y corresponding to that used in sections 4 and 5. The analysis in this section is for a two-layer ocean only. The extension of the ideas to more levels is in principle simple but in practice leads to very complicated equations and is unlikely to introduce more effects than those found in the simple two-layer model.

Consider a two-layer ocean, depths H_1, H_2, density ρ_1, ρ_2, where $H_2 \gg H_1$, $\rho_2 > \rho_1$. In the absence of topography, modes could be defined

$$\begin{aligned} \tilde{u} &= u_1 + \alpha_1 u_2 \\ \hat{u} &= u_1 + \alpha_2 u_2 \end{aligned} \qquad (35)$$

where α_1 and α_2 are the solutions of

$$\frac{H_1}{H_2}\alpha^2 + \alpha\left(\frac{H^1}{H_2} - g'/g - 1\right) - 1 = 0 \qquad (36)$$

which are approximately

$$\begin{aligned} \alpha_1 &= H_2/H_1 \\ \alpha_2 &= -1 + g'/g \end{aligned} \qquad (37)$$

where $g' = [(\rho_2 - \rho_1)/\rho_2]/g$. The first root corresponds to the barotropic mode and the second to the baroclinic mode. If we now consider topography of height T, then although the equations do not now decouple, we can still formulate them in terms of $\tilde{u}$, $\hat{u}$. Then we obtain

$$\hat{u}_{xxt} - \left\{l^2 + \frac{f^2}{gH_2[1 - (T/H_2)]}\right\}\hat{u}_t + \beta\hat{u}_x + \frac{Tf^2}{g'H_1(H_2 - T)}\hat{u}_t - \frac{ilf(\tilde{u} - \hat{u})T_x}{(H_2 - T)} = -l^2 X \qquad (38)$$

$$\hat{u}_{xxt} - \left(l^2 + \frac{f^2}{g'H_1}\right)\hat{u}_t + \beta\hat{u}_x + ilf\frac{H_1}{H_2}\frac{(\tilde{u} - \hat{u})}{(H_2 - T)}T_x = -l^2 X \qquad (39)$$

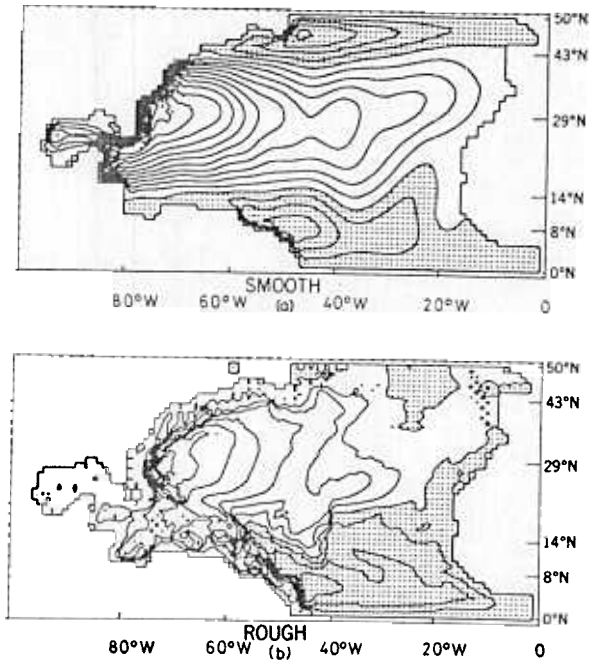

Fig. 3. Plot of the streamfunction after 100 days for (*a*) experiment 1 and (*b*) experiment 2. The position of the extrema in the forcing and its derivative are marked. The contour interval is 2 Sverdrups.

In the above, it is assumed that the topography does not intersect the density interface. This restriction is reasonable, for typically $H_1 \sim 500$ m, and apart from shallow continental slopes there are no significant areas of the North Atlantic where this would be invalidated.

Equations (38) and (39) should be compared with (8) for the case of no topography and with (31) for the response of a homogeneous (barotropic) ocean with topography. Equation (38) differs from (31) in the presence of the additional term $ilfT_x\hat{u}/(H_2 - T)$. Since $\hat{u}$ is of the same order as $\bar{u}$ (the Sverdrup balance is exactly the same for both $\bar{u}$ and $\hat{u}$), this means that the baroclinic field will significantly modify the barotropic response. On the other hand, the barotropic response has an order $H_1/H_2 \ll 1$ weaker effect on the baroclinic response (39). Thus there will be much less adjustment in the baroclinic field as a result of barotropic forcing. Likewise, the direct topographic effect $ilf(H_1/H_2)[T_x\hat{u}/(H_2 - T)]$ will be weak in the baroclinic case (though not totally negligible), but in contrast the effect on the barotropic response is a factor H_2/H_1 larger where $H_2/H_1 \gg 1$. Thus the barotropic mode will show a topographically influenced response on its own rapid time scale but will also change on the much slower time scale of the baroclinic mode, while the baroclinic mode essentially responds only on its own time scale.

We will now analyze the results of the numerical calculations and determine to what extent the simple theories of section 2 are appropriate. In the next section we will compare the results of experiments 1 and 2 and defer the comparison of the baroclinic results to later sections.

3. Barotropic Model Intercomparisons

a. Steady State Solutions

Because the barotropic planetary waves have high wave velocities, most of the adjustment of an ocean basin with no vertical density gradient can occur in the order of a few days, though some transient features last considerably longer. We will first analyze the solution after 100 days and then consider the transients. In Figure 3*a* the stream function is plotted after 100 days for experiment 1 (i.e., when there is no bottom topography). There is a well-established western boundary current of strength 30 Sverdrups, being part of the main anticyclonic circulation. In addition, weaker cyclonic circulations exist to the north and south of strength ~8 Sverdrups. In Figure 3*b* the corresponding stream function for experiment 2 is given. Figure 4 shows the topography used in this latter experiment. The inclusion of topography has led to a marked reduction in the strength of the western boundary current: the Gulf Stream transport is now only 14 Sverdrups. This result, namely, that for the homogeneous case topography weakens the circulation, is well known [see *Schulman*, 1975]. It follows as a consequence of (34).

Neglecting the divergence term p_t in (5) and introducing a stream function ψ such that $u = -\psi_y$, $v = \psi_x$, allows (8) to be written as [*Longuet-Higgins*, 1964]

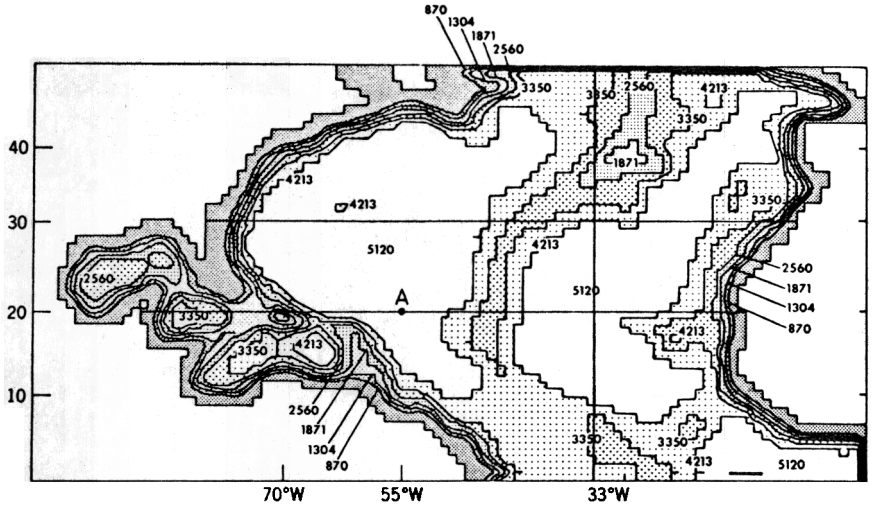

Fig. 4. Plot of the topography used in experiments 2 and 4. Figures give depth in meters and correspond to model levels. Contours shallower than 870 m have not been drawn. Solid horizontal and vertical lines indicate where time series sections have been taken (see, for example, Figures 5, 6, etc.). Point A gives the geographical location of the point where the spectrum of Figure 14*a* was taken for experiment 3.

$$\psi_{xxt} - l^2\psi_t + \beta\psi_x = -X_y \qquad (40)$$

The wind forcing has zero y derivatives at 14°N and 43°N (see Figure 1), and these positions have been marked on Figure 3*a*. The stream function when averaged across the basin is very nearly zero along these lines. The latitudes of zero curvature in X are 8°N and 29°N. These latitudes are marked on Figure 3*a* and again are in excellent agreement with the position of maximum ψ, though there is a tendency for the maximum of ψ to be displaced further north with longitude eastward, which could be an eastern boundary effect. There is a further maximum of $|\psi|$ at 46°N which does not correspond to any position of zero curvature in X but results from the fact that ψ has a zero at 43°N, is constrained to be zero at the northern boundary 50°N, and is forced by the wind in this range. Thus there must be a maximum of $|\psi|$ in this range.

Figure 3*b* shows qualitative features similar to those above. There is a region in low latitudes where ψ_y has a maximum at about 6°N (1° further south than in the flat case) and a large region in the interior centered on 29°N in which the general features are similar. At 45°W, 12°N there is a large latitudinal displacement of the flow, the so-called displaced gyre effect of *Schulman and Niiler* [1970] associated with the flow following f/H lines. The east-west gradients in this region suggest strong southerly flow at the east side of the ridge. The northern gyre is very different: the stream penetrates further north before separating from the coast and essentially destroys the northern gyre.

In the topographic case the latitude of a steady state zero streamline need not be independent of longitude, since topography can induce longitudinal variations. In the flat case such a variation can indicate effects of transients. Thus the large meander of the zero streamline in the east near 14°N (Figure 3*a*) may be indicative of transient behavior, and we will now examine this aspect.

b. *Transient Response*

In this section we will examine the transients of the solution and the mechanism by which the flow pattern shown in Figure 3 is established. There are two possible approaches, the basin mode approach and the wave approach. We will consider both.

Longuet-Higgins [1964] has analyzed basin modes for a flat ocean in simple closed geometry. These modes are defined as solutions which have a fixed frequency of vibration, the possible values being the eigenvalues of the problem. If we consider the simple case of an open middle latitude channel with straight north-south boundaries at $x = \pm L$, then the modes have frequencies given by (33), and the solutions of (32) are

$$\phi(x) = \sin\frac{n\pi(x + L)}{2L} \qquad n = 2, 3, \qquad (41)$$

Equation (33) has solution for both positive and negative ω for the same eigenfunction. Thus the resultant solution has components of the form

$$\psi = \exp[i(ly + \omega t + \beta x/2\omega)\sin\frac{n\pi(x + L)}{2L} \qquad (42)$$

and

$$\psi = \exp[i(-ly + \omega t + \beta x/2\omega)]\sin\frac{n\pi(x + L)}{2L} \qquad (43)$$

Equation (42) is the equation of a modulated wave traveling westward and southward and (43) that of a modulated wave

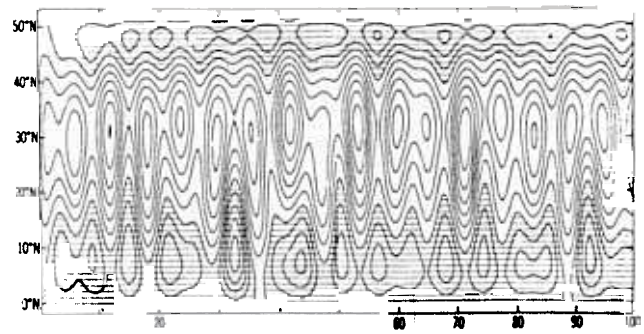

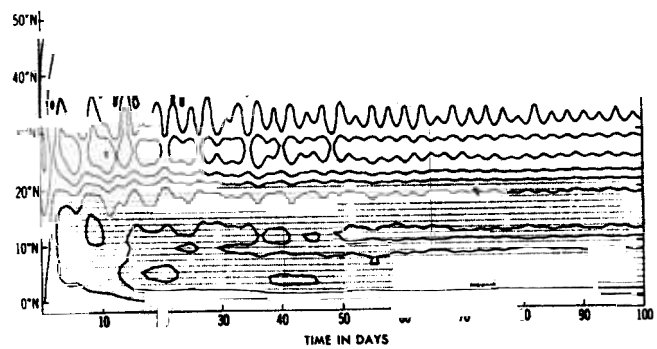

Fig. 5*b*. Same as Figure 5*a* but for experiment 2. The position of the section is marked in Figure 4. Note that the contour interval is the same (2 Sverdrups) as that for experiment 1, but the response is much weaker. The oscillations are at higher frequency than those in Figure 5*a*, more localized and damped out more rapidly.

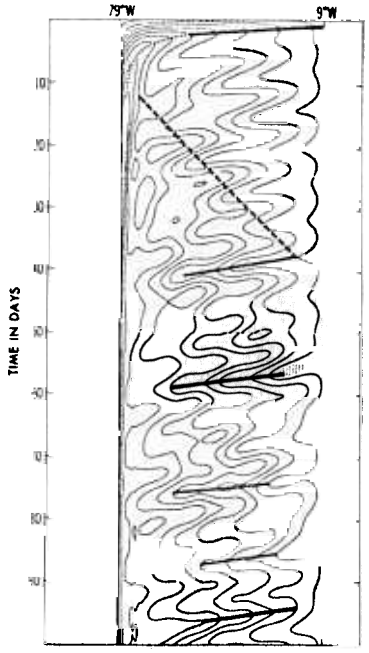

Fig. 6*a*. Contour of the streamfunction along 30°N against time for experiment 1. Phase lines appropriate to long Rossby waves (speed equals β/l^2) have been indicated (solid lines). The slope of the group velocity of the fastest short Rossby waves ($\beta/8l^2$) has been indicated by a heavy dashed line. While phase propagation appropriate to long Rossby waves is evident, that due to short Rossby waves is less well defined. The dotted line indicates the formation of the western boundary layer (see (14)). The contour interval is 3.5 Sverdrups.

mode to be in phase longitudinally over a large part of the basin with phase increasing linearly westward, consistent with the exp ($i\beta x/2\omega$) factor in (42) and (43). Further, the mode seems to have maximum amplitude at 30°N (see Platzman Figure 4), though the maximum in our case is further east. There is no evidence for Platzman's amphidromic point near 47°N in our results, though the presence of an artifical boundary at 50°N will have an effect on our results in this region.

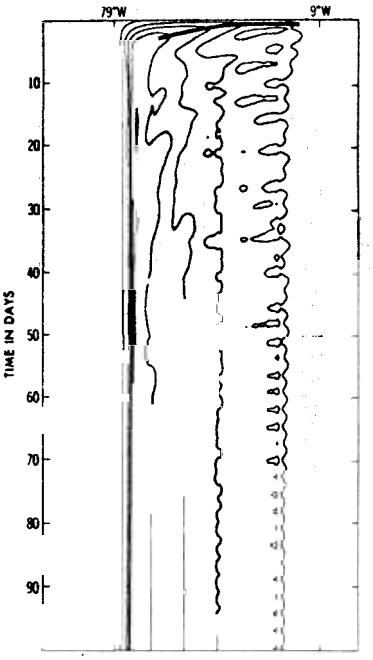

Fig. 6*b*. Same as Figure 6*a* but for experiment 2. In this case, no wave propagation is evident. The initial spin-up resembles that of Figure 6*a* but is slightly more rapid. The flow is weaker everywhere and becomes essentially steady within a period of the order of 30 days. The contour interval is 3.5 Sverdrups.

Figure 5*b* is the corresponding diagram for the topographic case. One notices the loss of coherence, the much reduced amplitude of the mode, and the significantly higher frequency. The inclusion of topography allows the modes to become more local in the sense that the function ϕ of (32) may be significant only in the vicinity of topography, with an essentially exponential damping away from the topography. Conjugate solutions of the form (42) and (43) no longer exist in the sense that it is not just l^2 which enters the problem. This means that coherence over all latitudes is more difficult to achieve. Nevertheless, Figure 5*b* does show that the oscillations are essentially in phase over all latitudes except around 35°N. (This can be more clearly seen when the contour interval is decreased. For comparison, however, the same contour interval is used as in Figure 5*a*.) Figure 4 shows that this is the region of strong topography variation where phase retardation is evident. The period of the oscillation is 2.6 days, somewhat longer than Platzman's lowest period (55 hours), which is maximum in the Grand Banks. There is no evidence in our results of such a maximum, so there seems to be little agreement between our results and Platzman's lowest mode. On the other hand, Platzman's second mode may relate more closely to the fundamental mode in our results, which is maximized on the northeastern part of the mid-Atlantic ridge.

In the above section we have shown the relevance, for this problem at least, of basin modes as a means of describing the transient solution. However, although the basin mode expansion can be shown to be complete, this does not imply that it is necessarily the best representation for all purposes. The solution can also be formulated in terms of planetary waves. *Anderson and Gill* [1975] used this approach to explain the middle latitude spin-up. In the barotropic case (see, for example, *Anderson and Gill* [1975], Figure 5) there are large perturbations to the steady Sverdrup solution caused by the waves. In this section we want to analyze our results to look for wave response and determine to what extent the solutions of section 2*b* are useful.

Figure 6*a* is a contour plot in time of the stream function along 30°N for experiment 1, while Figure 6*b* is the corresponding plot for experiment 2. In Figure 6*a* there are several places where phase lines slope linearly downward from right to left. If these indicate long Rossby waves, the phase slope should correspond to a speed of β/l^2. Examining Figure 1 shows that l varies with latitude and that no specific value of l can really be ascribed.

A value of $l = 10^{-6}$ m^{-1}, however, seems a reasonable compromise. For this value the planetary wave speed is 20 m/s, which is in reasonable agreement with the observed slopes. A solid line with slope appropriate to this speed has been drawn in Figures 6*a* and 7. *Anderson and Gill* [1975] have examined the spin-up of ocean with boundaries aligned north-south and shown how the long waves can be expected to alter rapidly the interior spin-up and set up a Sverdrup balance from the eastern boundary. In the western boundary region the phase lines should slope downward during the initial adjustment period associated with the Bessel function behavior of the short Rossby waves (see (14)). Such behavior is clearly evident in Figure 6*a* in the initial phase.

At all times there appears in Figure 6*a* to be wavelike behavior across the basin, but it is not in general possible to

pick out coherent behavior. At different latitudes these eastward moving wave trains can be more evident. For example, in Figure 7 we plot the streamfunction at 20°N. There are several places, particularly between days 10 and 40, where such trains exist. They are marked by the dashed lines. The slope of this line appears to be 8 times that of the westward moving waves (solid lines). This is consistent with these being eastward waves with the fastest group velocity, but no good reason is offered for why we apparently get this intermittent wave train behavior.

In the case of Figure 6*b* the initial spin-up is faster than in the flat bottom case, but the phase lines deviate from a straight line. This results from the fact that the analog to (8) when topography is included is (31). The presence of the $ilfT_x/H(1 - T/H)$ term makes a plane wave solution inadmissible, as this term is a strong function of x. Figure 6*b* also shows the presence of basin modes just east of the ridge. The wave propagation is rapidly damped out in Figure 6*b*, and the solution adjusts to the (topographic) Sverdrup solution more rapidly than in the flat bottom case. This is presumably because topography breaks up the flow into smaller-scale features which can than be dissipated more rapidly (a scale selective damping term ($K\nabla^2$) is used in the momentum equations). It should be emphasized that the high-frequency oscillations evident in Figure 6*b* are real. They are not numerical noise. Their period is 2.6 days, corresponding to 26 time steps, and so they are well resolved by the model. The rapid reduction in period of basin modes with increasing topography has been analyzed by *Anderson and Killworth* [1977] and *Ripa* [1978] motivated by these results. It is shown by these authors that it is primarily the lowest basin mode for $\pm l$ which responds strongly to topography, and this is usually the mode most excited.

In conclusion, we would deduce that for the no topography case the basin mode formulation, where the solution is envisaged as a sum of modulated waves, and the conventional Fourier analysis, where the solution is considered as a sum of plane waves, are both appropriate and useful methods for considering the large-scale adjustment. Basin mode analysis gives a good idea of the frequencies of the response, while wave analysis gives a clearer picture of the initial adjustment. When multiple reflections occur, neither method has a clear advantage. When topography is included, the basin mode method remains applicable, whereas the plane wave method is, strictly speaking, inappropriate, though for certain situations it can remain a useful tool.

Although this section applies strictly to a homogeneous fluid, some of the results should be applicable to the stratified case also. This is because the additional modes of adjustment possible when stratification is present are slow in comparison with the barotropic adjustment. Thus in a stratified ocean we would still expect it to adjust in the barotropic mode (for short times) in much the same way as in this section. Thus the tendency for energy to be concentrated at certain (basin mode) frequencies should apply. These modes we would expect to be excited whenever there is a rapid large-scale adjustment in the wind field. The results of experiment 2 indicate however that the western Atlantic is not a good region in which to observe basin modes, since they have little amplitude there. This may explain why they have not yet been observed. B. Zetler (private communication, 1976) has studied high-resolution spectra for adjusted sea level at Bermuda but finds no significant peaks of periods appropriate to basin modes.

4. Early Stages of Baroclinic Development: The First Month

a. Equatorial Adjustment

In a stratified ocean, in addition to the rapid response to the external mode, there is also the slower response of the baroclinic modes. Near the equator, however, these can respond reasonably fast. For example, the first baroclinic planetary wave can cross the equatorial Atlantic in approximately 65 days, while at middle latitudes it takes several years. In addition to the rapid equatorial response, there can be rapid coastal response. At the western boundary, coastal Kelvin waves traveling equatorward can excite equatorial Kelvin waves. These in turn excite poleward traveling coastal waves at the eastern boundary [*Moore*, 1968]. The extent to which these various effects are present in a realistic ocean will be examined.

It is convenient to analyze the behavior in terms of vertical

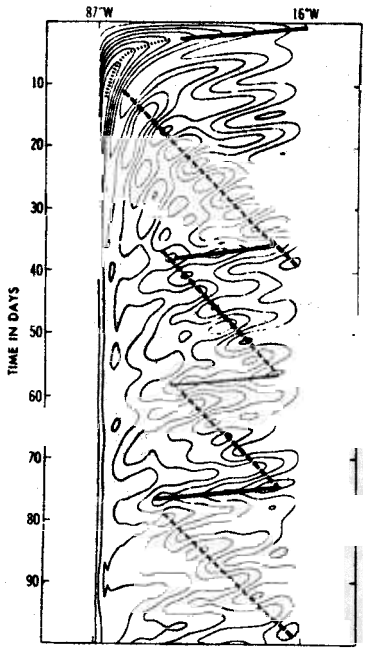

Fig. 7. Same as Figure 6*a* but along 20°N for experiment 1. In this case, not only is the phase propagation of long waves evident, but there also appear to be wave trains with slopes appropriate to short dispersive waves. The contour interval is 3 Sverdrups.

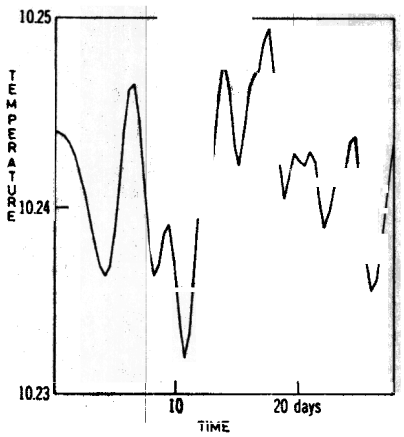

Fig. 8*a*. Equatorial temperature record at (33°W, 0°N) at a depth of 1087 m (model level 7).

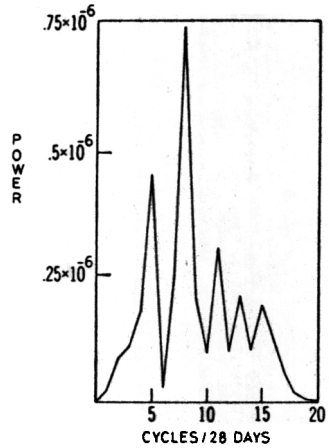

Fig. 8*b*. Power spectrum of the time derivative of the record of Figure 8*a*. The horizontal axis corresponds to the number of cycles per 28 days.

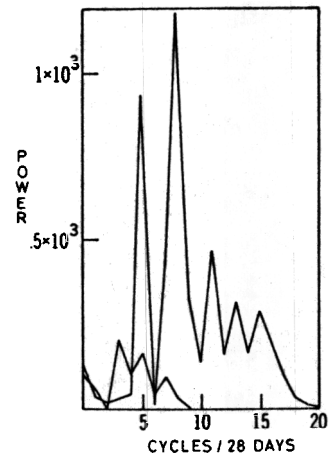

Fig. 9*b*. A plot against frequency of the power spectrum of the time derivative of the modal amplitude for the records of Figure 9*a*. The upper curve corresponds to the first mode, the lower to the second mode.

modes (2). The density field used was that of a typical mid-Atlantic profile, being related to temperature by the simplified equation of state

$$\rho = \rho_0(1 - \alpha T) \tag{44}$$

The temperature at the 12 model levels are given in Table A1 of Appendix A. Salinity effects are not included.

Since there is no interaction between the modes, the external or barotropic mode should behave exactly as in experiment 1 in the previous section, and so we shall concentrate on the baroclinic response here, beginning with the equatorial response. Since the initial equatorial and coastal response under consideration is rapid, the results of this section are for a short experiment of 28-days duration, started impulsively at day zero with a wind of the form (1).

In the absence of boundaries, each mode will be excited at a variety of frequencies given by (24), corresponding to gravity inertial waves of zero wave number [*Wunsch and Gill*, 1976]. For the first two modes, c_1 = 2.71 m/s and c_2 = 1.3 m/s. This means that in a record of 28 days we would expect to see oscillations as given in Table 2. Only symmetric modes appear, as reflectional symmetry at the equator has been imposed. In Figure 8*a* a typical temperature record is plotted for a point at 0°N, 33°W (in this case at a depth of 1087 m) and the power spectrum of the time derivative is given in Figure 8*b*. (The technique of differentiating the record before spectral analysis was often found useful for filtering very low frequencies. Note, however, that it gives additional weight to the higher frequencies.) The record appears rather complicated but can be explained simply if we make a decomposition into modes. In Figure 9*a* the record for modes 1 and 2 based on the depth-integrated temperature field (i.e., pressure) is plotted, and the power spectra are given in Figure 9*b*. The main periodicities in Figure 8*b* and Figure 9*b* are the same. In fact, they are in reasonable agreement with Table 2, with peaks at 5, 8, and 11 cycles/28 days for mode 1. The sampling frequency is 4 days, so some aliasing may be involved in the higher frequencies. For mode 2 there are peaks at 3, 5, and 7 cycles/28 days but no higher frequencies, suggesting that they are only weakly excited or that the model damps them out.

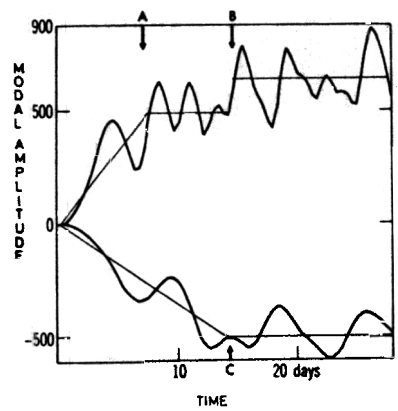

Fig. 9*a*. A plot of the amplitude of the first (upper) and second (lower) modes as functions of time for a point on the equator at 33°W. Points A and C indicate the arrival of the Kelvin waves and fastest gravity inertia waves from the west coast for modes 1 and 2, respectively. For times less than this there is a linear increase with time, with inertial oscillations superimposed. For later times, boundary effects become important and induce a response which is steady (apart from inertial oscillations). Point B indicates the time at which gravity inertial waves from the east coast arrive at 33°W for the first mode. Such waves do not arrive within the time scale of the graph for mode 2.

In addition to the gravity inertial oscillations there are many other modes of propagation of equatorial waves. These are summarized in section 2*c*. To isolate these waves, the amplitude of pressure modes 1 and 2 are contoured in Figure 10*a* and Figure 10*b* in *x-t* space. The section is along the equator from the South American coast to the African coast. In the interior there is a linear spin-up modified by the inertia gravity waves of zero wave number discussed previously. Propagating in from the western boundary at speed c = 2.71 m/s is the equatorial Kelvin wave and gravity inertia wave. There is essentially no disturbance to the interior flow eastward of this line. At the same time traveling westward is another inertia gravity wave. However, there is some disturbance west of this

TABLE 2. Frequencies of Equatorial Inertial Oscillations for the First and Second Baroclinic Modes

Order m of Parabolic Cylinder Function	Number of Periods in 28 Days	
	Mode 1	Mode 2
0	5.0	3.6
2	7.7	5.5
4	9.7	6.9

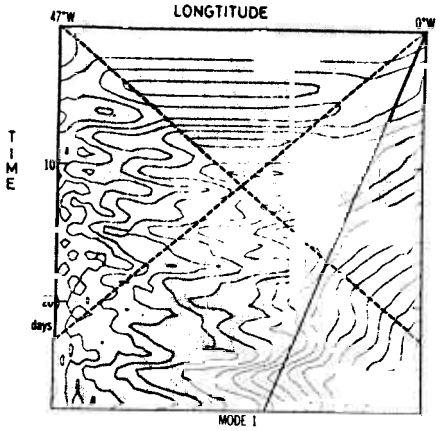

Fig. 10*a*. Contour of the amplitude of the first pressure mode along an equatorial section from 47°W to 0°W. Dashed lines indicate the propagation of the fastest gravity inertia wave (and Kelvin wave in the case of eastward propagation from the west coast), while the solid line corresponds to the fastest planetary wave (which travels at 1/3 the above speed). Note the pressure gradients set up by the Kelvin and planetary waves.

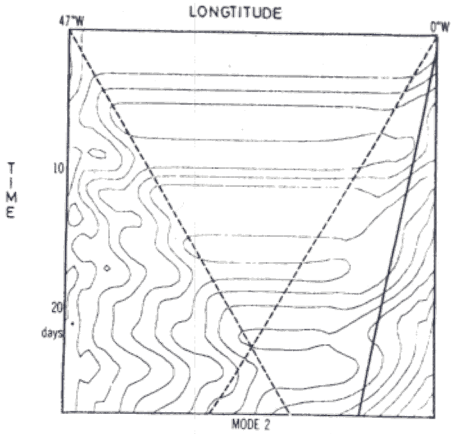

Fig. 10*b*. Same as Figure 10*a* but for pressure mode 2.

wave front. In a geometry with straight north-south coasts there are no waves which could give rise to such an effect, but for the geometry used here propagation of this nature is possible, since gravity inertia waves of speed c can propagate north-south from the Gulf of Guinea. *Philander* [1977] has also shown there would be some interaction between coastal and equatorial waves in the Gulf of Guinea, since the scales are slightly overlapping. However, the interaction on the equatorial response is extremely weak. In the wake of the inertia gravity wave front there are westward traveling planetary waves at speeds $c/3$, $c/7$, $\cdots$. The phase line for the first of these is drawn. Eastward of this a pressure gradient (or temperature gradient) is established. Planetary waves are not alone in establishing a pressure gradient. The Kelvin wave also establishes a pressure gradient in the same direction as the planetary wave. Figure 10*a* indicates that the pressure at the western boundary becomes independent of time after a short spin-up phase (apart from inertial oscillations), and thus the pressure in the interior will become time independent after the Kelvin wave has past and before any significant eastern boundary influence is felt.

In Fig. 10*b* the equatorial response in the second mode is plotted. The features indicated in Figure 10*a* again occur but at a slower speed. Because of this it is easier to see the effects of the various waves as they are more clearly separated in time.

Returning to Figure 9*a*, which is a time plot of modal amplitude at a given equatorial point, we can see how the interior solution spins up until the Kelvin wave arrives (points A and C for modes 1 and 2, respectively) and remains steady (apart from inertial oscillations) until the first wave from the east arrives (point B) for mode 1. Mode 2 does not experience eastern boundary effects at this point within the time span of the experiment. We will now consider coastal response.

The wind can produce a local response where there is a longshore wind [*Charney*, 1955]. The resulting upwelling or downwelling can propagate as a coastal Kelvin wave along the coast (see (16)) [*Csanady*, 1968]. In addition to local coastal forcing, coastal Kelvin waves can be excited by equatorial Kelvin waves. *Moore* [1968] and *Anderson and Rowlands* [1976] have examined this process in some detail for the time harmonic case and spin-up case, respectively. *Hurlburt et al.* [1976] have also shown numerically the dramatic relaxation that occurs when the wind is switched off. *Godfrey* [1974] has also considered the spin-down problem. All the above work has been for very idealized oceans. To illustrate the existence of such waves in our model and to show the effects of propagation on the local response, a coastal section was contoured as a function of time. This is shown in Figure 11 for pressure mode 1. It represents a continuous strip following the perimeter of the model basin with the equatorial section in the middle, then moving right we have the coastal values round the Gulf of Guinea and along west Africa. The part toward the right where there are horizontal contours corresponds to the artificial boundary at 50°N. Then we proceed down the east coast of North America. Moving to the left side of the figure we continue down North America back to the equator. The merit of this diagram is that it gives an almost linear coastal record (not quite linear because the values are at grid points which are 1° apart in latitude and longitude and the longitudinal separation therefore decreases slightly as we go north). Contour lines

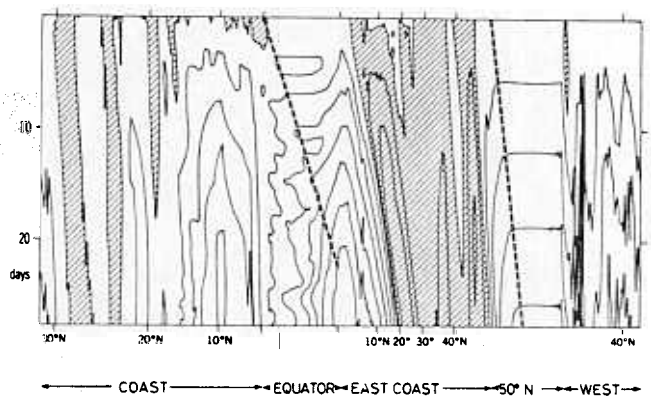

Fig. 11. Amplitude of pressure mode 1 on the basin perimeter as a function of time. All coastal amplitudes have been mapped onto a continuous strip. Left to right in the diagram corresponds to going round the basin perimeter anticlockwise. The equatorial zone is marked near the center of the diagram. To the right of this is the eastern boundary, from the Gulf of Guinea, round the African coast to 50°N. Then we have the artificial boundary at 50°N. This is followed by western boundary amplitudes. These are continued on the left of the diagram. Heavy dashed lines indicate observed Kelvin wave speeds along the equator and the artificial boundary at 50°N. Strong coastal propagation is also evident in the 0°-20°N range on the east. The increase in gradients in this region is due to the Kelvin wave traveling into a thinning wave guide as the radius of deformation c/f decreases with increasing latitude.

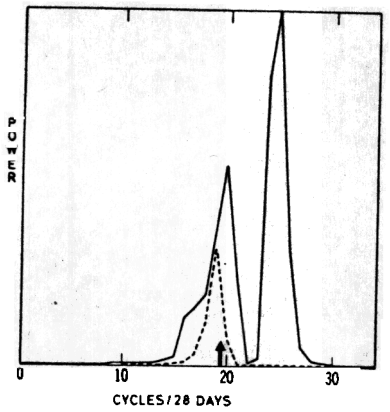

Fig. 12*a*. Power spectrum of the time derivative of the amplitude of pressure modes 1 and 2 at an interior point (55°W, 20°N) (see Figure 4). The heavy arrow indicates the local inertial frequency. For mode 1 (solid curve) there is energy at a higher frequency, while for mode 2 (dashed curve) the energy is located only near the inertial frequency.

going vertically indicate that the modal amplitude there is stationary. Horizontal lines indicate uniform response, and sloping lines can result from propagation or from variation in the local response either because the magnitude of the wind stress varies with latitude or because the angle between the wind and the coast varies. The equatorial section has already been discussed. Just to the right of this one can see two effects. Along the Guinea coast where the wind is parallel to the coast, one would expect the amplitude of the mode to increase linearly with time (corresponding to downwelling). This increase is evident but not spatially uniform. This is due to the passage of a coastal Kelvin wave along the coast away from the equator. The wave is excited by the equatorial response and results in the downwelling found at 10°–20°N in the first few days being changed to upwelling by the end of a month. It is also evident that the longshore gradients at the head of the Kelvin wave are increasing with time. This results from the fact that the radius of deformation reduces rapidly as one goes north from ~215 km at the equator to 55 km at 20°N. The speed of passage of the wave is such that it essentially maintains its energy and thus its amplitude increases, implying strong gradients in the vicinity of the head of the disturbance [*Anderson and Rowlands*, 1976].

Other propagation effects are visible. For example, the wave traveling along the artificial boundary at 50°N. Theoretically, the Kelvin wave should travel with uniform speed c regardless of latitude. This means that the slope of the phase line at 50°N should be somewhat less than that at the equator or along the coast of Guinea, since 1° of longitude at 50°N is only 65% of that at the equator. In fact, the slope of the phase line at 50°N is larger than that at the equator. This is a numerical problem. The radius of deformation decreases with increasing latitude to 25 km at 50°N. But the model resolution is only 1°. Thus at increasing latitude the ability to resolve the radius of deformation decreases, and as is shown in Appendix B, this leads to a phase retardation. Figure 11 shows one further interesting result: the apparent almost total lack of propagation effects at the western boundary. At the west a Kelvin wave propagates equatorward into an increasing radius of deformation, and gradients thus decrease. This makes it harder to detect. In addition, at the east the coastal Kelvin wave is forced by the equatorial Kelvin wave which can be quite large. For both these reasons, coastal propagation is enhanced at the east over that at the west.

b. Interior Adjustment

Short-term interior adjustment takes place mainly via inertia gravity waves. Following the switch-on of the wind, inertial oscillations are excited in the ocean interior. The frequency of these oscillations is higher at higher latitudes. In Figure 12*a* the spectrum of the time derivative of the temperature at a midocean point is given. There is a large peak at the local inertial frequency but also at a higher frequency.

In Figure 12*b* the spectrum of the velocity field obtained by integrating (29) is plotted. No zonal variations are involved in producing this diagram. The increase in frequency is associated with β dispersion, the propagation of energy equatorward from a region in which the local inertial frequency is higher [*Anderson and Gill*, 1979].

In Figure 13 the amplitude of the pressure mode 1 along the section at 33°W is plotted as a function of time. The rapid adjustment from positive to negative amplitude near 15°N (the latitude where $(fX)_y$ is zero) at the beginning is accomplished by gravity waves. The adjustment at this time can be reproduced with a model set of equations pertaining to a boundary at y = 50°N and 0°N with no x variation, indicating this effect is not associated with longitudinal propagation. Note in Figure 13 the linearly increasing upwelling at the northern boundary constrained to the narrower boundary scale than the corre-

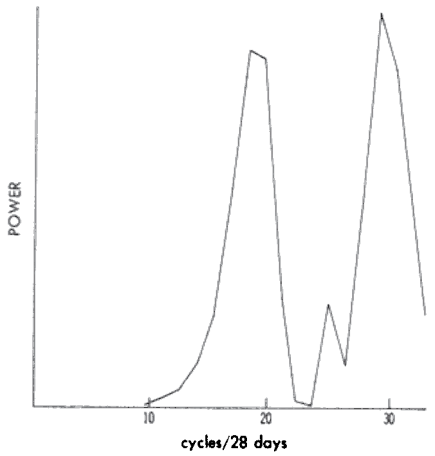

Fig. 12*b*. Power spectrum of the amplitude of velocity mode at 55°W derived from integrating (29).

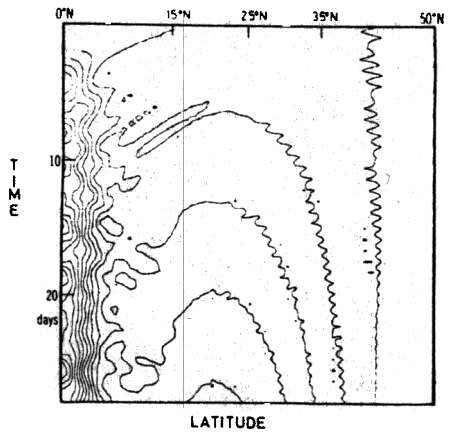

Fig. 13. Contour plot in time of the amplitude of pressure mode 1 along a section at 33°W from the equator to 50°N. This figure should be contrasted with Figure 2*b*.

sponding solution near the equator. The equatorial upwelling does not continue to increase as an equatorial Kelvin wave from the western boundary soon reaches the longitude of this section.

5. BAROCLINIC MODEL INTERCOMPARISONS OVER 1600 DAYS

a. Transport Streamfunctions

Having analyzed the short-term response (28 days), it is now instructive to look for longer-term effects when propagation is not restricted to coastal regions and the equator. We will consider two long (1600 day) runs: flat stratified ocean, experiment 3 (which is essentially a continuation of section 4), and stratified ocean with topography appropriate to the North Atlantic, experiment 4. The vertical stratification in experiment 4 is identical to experiment 3 and is homogeneous in the horizontal. The topography used is the same as that in the barotropic experiment (section 3).

In experiment 3 the vertical modes are all decoupled, and each adjusts to its own equilibrium on its own time scale, which is rapid for the barotropic modes and gets progressively slower for the higher baroclinic modes. The fact that the modes are decoupled means that the streamfunction in experiment 3 is the same as it would be in an extension of run 1. At 100 days the two streamfunctions are the same to within a small numerical accuracy. Thus using the knowledge of section 2*b*, we can expect most of the adjustment in the streamfunction in the stratified case to take place within a few days but for basin modes to persist for a longer period. In Figure 14 the streamfunction across the basin at 30°N is plotted for 1600 days. This shows that basin modes are damped out on the time scale of 6–9 months.

In contrast, when topography is included, the modes are neither independent nor free to adjust to their own equilibrium on their own time scale. The lower diagram of Figure 14 (rough) is a contour plot for experiment 4 of the variation of the streamfunction along 30°N with time, for comparison with the upper diagram for experiment 3. When topography is included, in addition to the rapid adjustment for small times, there is a much slower adjustment on the time scale of the baroclinic modes. It was this and subsequent results which prompted the analysis by *Anderson and Killworth* [1977]. As shown by (38), the barotropic mode is affected directly by the topography and also indirectly by the baroclinic mode. Equation (38) is a model equation to indicate how topography can affect the streamfunction and the time scale of the adjustment. In the numerical model there are 12 levels, not two, as used to deduce (38), and the topography used is different. Thus no direct comparison exists between Figure 10 of Anderson and Killworth (obtained by using (38)) and Figure 14 (rough). Nevertheless, a certain similarity does exist. In both diagrams, basin modes can be seen initially, though they are damped out much more rapidly in Figure 14. (For Figure 14 a scale selective damping is used, i.e., $K\nabla^2$ dissipation, whereas for Figure 10 of Anderson and Killworth only bottom friction was used.) There is a slow adjustment in both diagrams to a state in which the balance is approaching the flat Sverdrup rather than the topographic Sverdrup.

Comparing Figure 14 (rough) with 14 (flat), one can see that the transport in the former at the end of 1600 days is 28 Sverdrups, almost as much as that in the flat case (30 Sverdrups) and considerably more than that after 100 days (16 Sverdrups). This effect can be more graphically illustrated by comparing Figure 15, the transport streamfunction after 1600 days in experiment 4, with Figure 3. It resembles much more closely the flat case (experiment 1) than the topographic case (experiment 2). Thus stratification allows the effects of topography to be reduced [*Anderson and Killworth*, 1977]. Many topographic features evident in Figure 3*b* have been ironed out

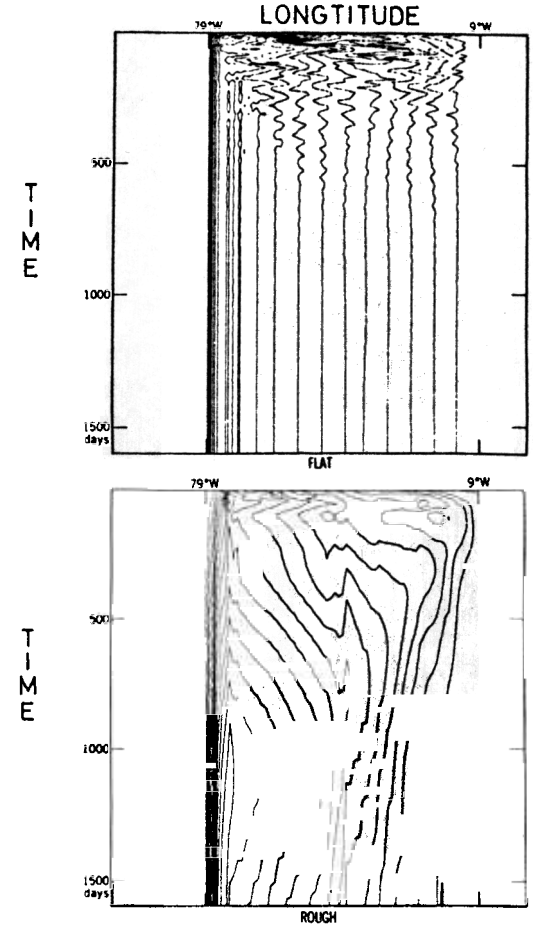

Fig. 14. Contour plots of the streamfunction along 30°N for the two stratified experiments 3 (flat) and 4 (rough). In experiment 3, all adjustment takes place near the beginning, with basin modes being damped out within ~250 days. For experiment 4 the basin modes are damped out within 50 days, but a much slower adjustment takes place throughout the whole 1600 days. The contour interval is 2 Sverdrups. Note that there are 16,000 time steps in the time span of this diagram and that the rapid oscillations (basin modes) are well resolved.

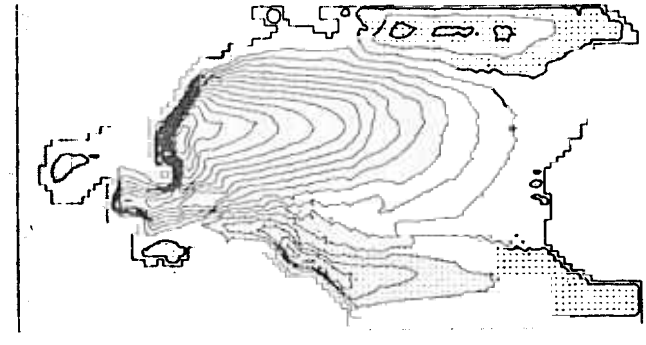

Fig. 15. Plot of the streamfunction after 1600 days for experiment 4. The contour interval is 2 Sverdrups. This figure should be compared with Figure 3. It resembles much more closely the flat case (experiment 1) than the rough case (experiment 2). This is because stratification allows the effects of topography to be reduced.

by the baroclinic modes. This has not happened everywhere because baroclinic adjustment is still taking place.

For example, adjustment is in fact still occurring in the Caribbean associated with a baroclinic wave front penetrating this region (see Figure 23). In the homogeneous case (Figure 3*b*) the Gulf Stream off Florida has, say, its maximum intensity some 5° from the coast, at the foot of the western shelf. This is in agreement with the analysis of *Schulman* [1975] for a homogeneous ocean, which showed that the current is expected to increase until the abyssal plain is reached. When baroclinic effects are included, the stream can ride up onto the shelf (as is observed), and in Figure 15 the maximum x gradient is attained approximately 2½° from the coast. There is an interesting adjustment along the Guiana coast also. The total transport in reversed in this area compared with Figure 3*b* and now resembles the no-topography case much more closely, except that the maximum transport is further north. Compared with Figure 3*b*, the southward current on the east side of the mid-Atlantic ridge at about 12°N has been removed. The separation of the Gulf Stream appears to be a little further south than it is in Figure 3*b*, but baroclinic adjustment is much slower in higher latitudes and the circulation of Figure 15 has not yet attained equilibrium in this area. At longer times it is expected to resemble Figure 3*a* in this area also.

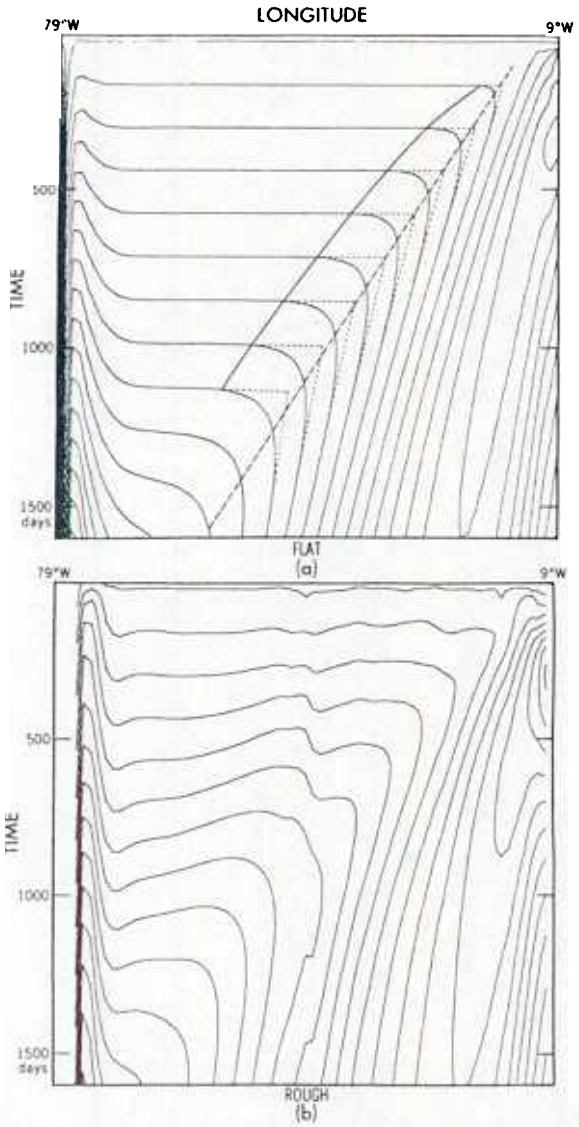

Figure 16. Same as Figure 14 but for temperature at level 7. The dashed line gives the theoretical propagation slope for Rossby waves (calculated from (11)). The solid line indicates the 'observed' deviation from a linear increase with time, indicative of precursors. Contour interval is 0.025°C.

b. *Temperature Response*

According to (39), the baroclinic mode feels the effect of topography much less than the barotropic typically by a factor $H_1/H_2 \sim 500/5000$ m = 0.1. Hence only a weak topographic effect is to be expected in the baroclinic case. This implies that a similar temperature response is to be expected in experiments 3 and 4. To test this, temperature sections across the basin at 30°N are plotted in Figure 16 for the two experiments. These figures are quite similar, indicating that the baroclinic field is only weakly affected by topography. Figure 16 shows an interior region in which the temperature increases linearly with time.

To the east of this interior region is a region affected by Rossby waves from the eastern boundary. The theoretical westward wave speed is

$$c_g = -\beta/(l^2 + f^2/c^2)$$

For latitudes higher than ~10°N the l^2 term is negligible. The planetary wave speed at 30°N is 2.74 cm/s for the first mode. In Figure 16*a* a dashed line with this slope has been marked. One can see that it gives a good measure of the intersect of the interior and postwave temperatures (indicated by the thin dashed lines). However, information is clearly traveling into the interior faster, as measured by the solid line. The nature of this precursor has been analyzed by *Anderson and Killworth* [1979]. It takes the form of a diffusive boundary layer traveling with the wave front. The agreement between the theoretical Rossby wave speed and the model wave speed was not always as good as it is in Figure 16*a*. Invariably the model speed was higher than the value predicted by the theory.

Returning to Figure 16*b*, one can see that the interior solution is not independent of longtitude as it was in Figure 16*a*. There is some distortion from the topography, but the main features are the same in both. There is no major readjustment as there was in the transport streamfunction (Figure 14). Locating the position of the long wave front cannot be so precisely done as in Figure 16*a*, but one can see clear evidence of its existence.

Equations (38) and (39) were deduced for middle latitudes. They do not strictly apply near the equator. However, one can see that the topographic terms are premultiplied by f. This suggests that the direct influence of topography is unlikely to be greater at lower latitudes. In Figure 17 we plot sections along the equator for the two experiments to show the relative similarity. To show the spatial nature of the temperature changes with time, the level 2 temperature is plotted in Figures 18*a* and 18*b* for 160 days and 1600 days. The response in middle latitudes is initially longitudinally independent, except near the boundaries and within a few degrees of the equator. The effects of equatorial and coastal dynamics in altering this pattern are fairly easily defined. There is an equatorial temperature difference of 3° between east and west, and eastern coastal propagation effects have displaced the 18° isotherm by 20° of latitude.

Figure 18*a* also shows strong coastal gradients along the Guiana coast. There is a stronger gradient there than in the Gulf Stream, suggesting stronger baroclinic currents. However, this is the picture after only 160 days. After that time the

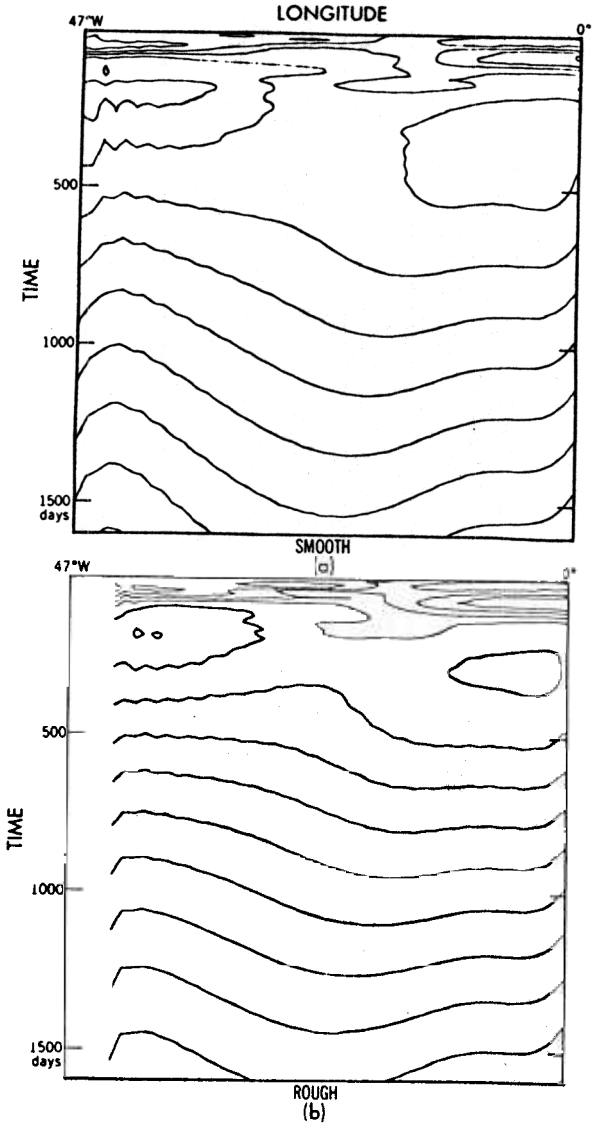

Fig. 17. Temperature at level 7 (1087 m) along the equator for (*a*) experiment 3 (upper) and (*b*) experiment 4 (lower) showing that the temperature fields are remarkably similar. Contour interval is 0.01°.

temperature gradients in the Gulf Stream increase more rapidly and by day 1600 (Figure 18*b*) are stronger. Propagation into the interior from the west is also well illustrated. The temperature front propagates at different speeds at different latitudes, which gives rise to an apparent northwestward component of movement.

The cooling in the eastern Atlantic is very marked. After 1600 days the surface temperature has fallen some 12° and is still cooling at a rate of 1.0°C/300 days. The center of the gyre is warmed by 2° over the whole period. All coastal points have cooled. The large equatorial disturbances suggest that nonlinear effects will be important in practice, although they have been deliberately left out in the present study. (In fact, in the eastern tropics the vertical temperature structure is markedly unstable, though this has no effect in a linear model.)

c. *Velocity Profiles*

In Figures 19*a* and 19*b* the surface velocity is plotted after 160 days and 1600 days, respectively, for experiment 4. At the earlier time the major current systems are the Guiana current and the south equatorial current (the flow westward on and north of the equator). The Gulf Stream is not yet well developed. During the next 1440 days the Gulf Stream intensifies, and the Guiana current in the lower latitudes dies away.

There is a weak eastern boundary current along the Spanish Sahara and Morocco which broadens westward and intensifies slightly. This current is mainly located where the wind has a substantial component parallel to the coast but also is maintained by coastal propagation effects, for there is a coastal current where the wind stress is zero and also where the coast is normal to the wind. In the Gulf of Guinea the surface flow is weak but opposite to the Guinea current. The south equatorial current, initially well developed, is not maintained and dies away with time. In Figure 20*a* the current at 160 days is shown at 160 m for experiment 4. Along the equator the flow is eastward as in the undercurrent, but there is no undercurrent near South America largely as a result of the northwestward Guiana current which is fed by the interior flow leaving little to feed into the undercurrent in this region. However, in the vicinity of 6°N the subsurface Guiana current undergoes a rapid readjustment and by day 300 has completely reversed and now is southeastward, a direction it continues to maintain until the end of the experiment (Figure 20*b*). This figure gives the impression that the undercurrent is fed to a large extent by this flow. The increase in the zonal flow with time evident in the surface current (Figures 19*a* and 19*b*) is also present here. It is also interesting to note the stagnation which occurs in the eastern Gulf of Guinea. The wind is parallel to the coast here and would, on a local argument, be expected to produce a local current. As Figures 20*a* and 20*b* show, no current develops indicating propagation effects associated with the equatorial adjustment. In Figure 20*a* there is a southward coastal current as far south as 10°N, but in Figure 20*b* this current has

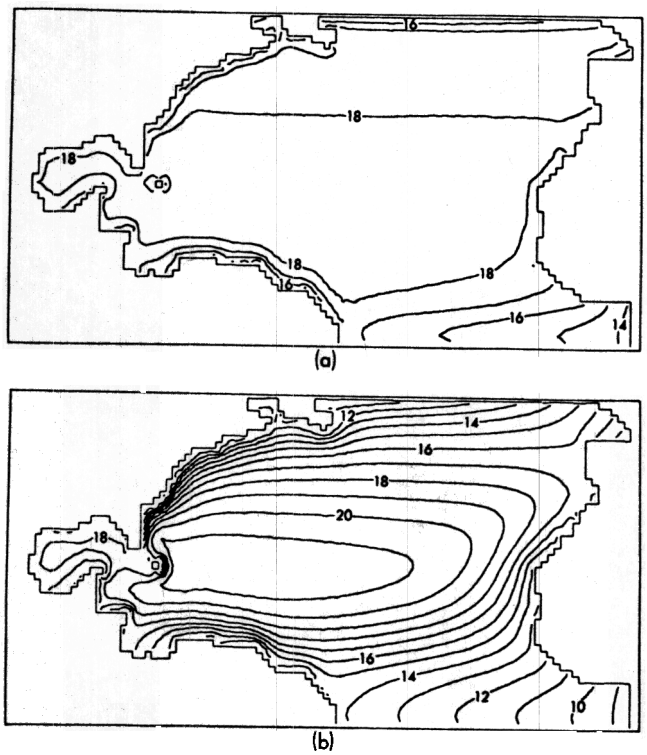

Fig. 18. Plot of the temperature at model level 2 for experiment 4 after (*a*) 160 days and (*b*) 1600 days. Initially, the temperature was uniform. After 1600 days all coastal points have cooled, while the interior has warmed. The contour interval is 1°C.

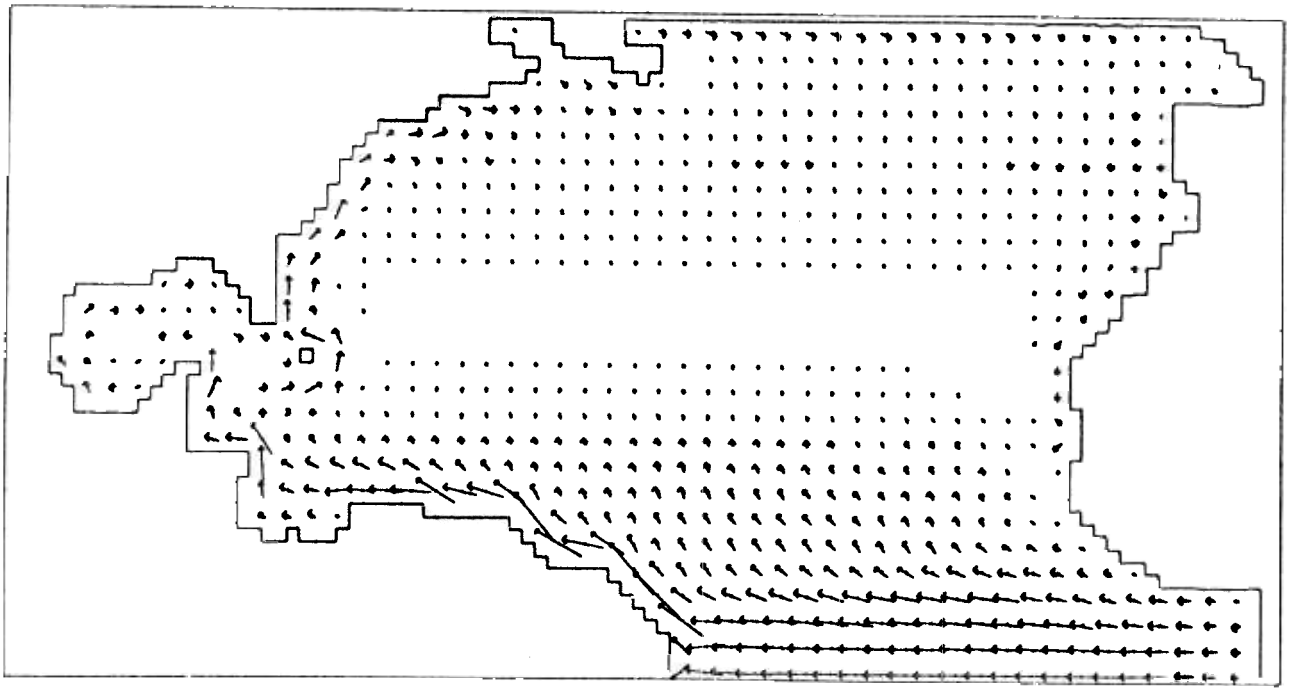

Fig. 19*a*. Surface velocity after 160 days. The main currents are along the Guiana coast and parallel to the equator at ~ 4°N.

broken away from the coast and becomes an interior current except along the Spanish Sahara and Morocco coast.

In Figure 21*a* we show the deep currents at 3350 m for experiment 4 after 1600 days. There is apparently quite a lot of structure to these currents, but the amplitude is small. This is not altogether unexpected, since the topography at 3350 m would be expected to produce significant effects at this level as the current flows around the ridges, etc.

However, the overall flow pattern in its broad characteristics is rather similar to Figure 21*b*, which is for the flat case. Details of currents particularly in the west are different. This is inevitable, as at this level in the rough case the coastal boundary is much further east. But the flow patterns in the two graphs remain the same. In the interior and toward the southeast the main current bands are the same. These are set up by the various baroclinic modes propagating toward the northwest. As was discussed previously, the coherence of these baroclinic modes is not destroyed by topography. The effect of

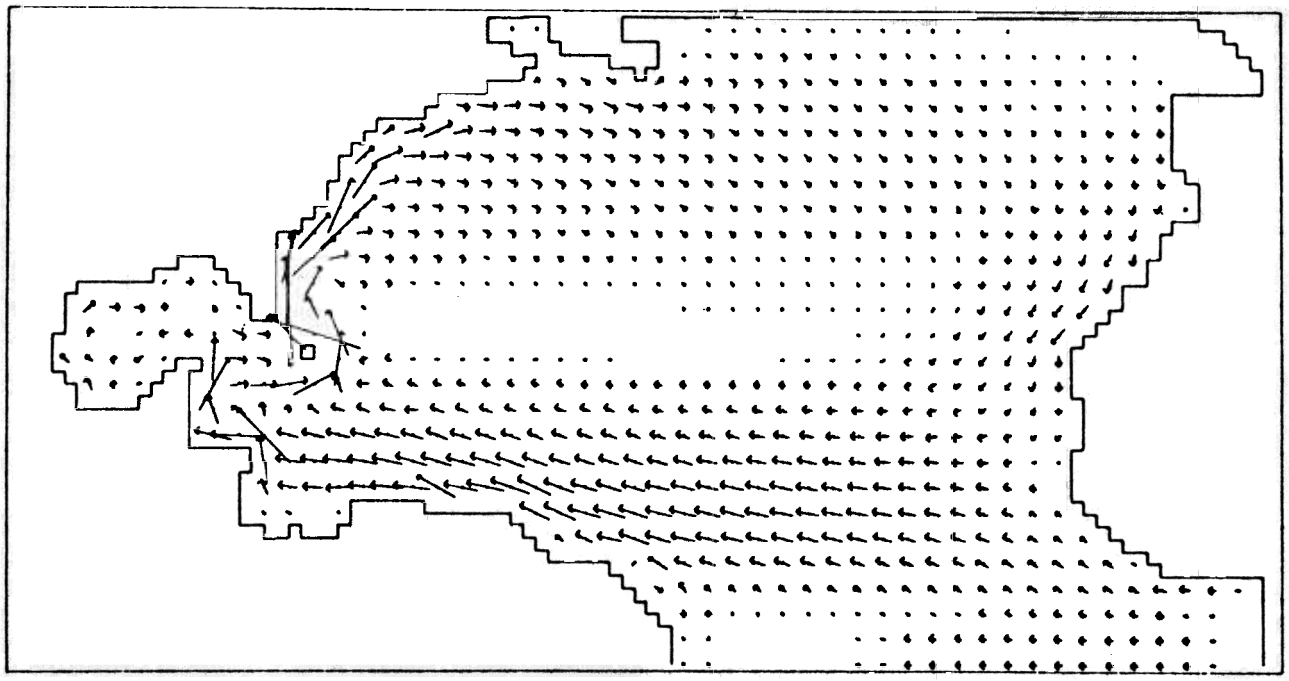

Fig. 19*b*. Same as Figure 19*a* after 1600 days. The Gulf Stream has intensified. The interior flow in the northern part of the basin has changed from being southward to east and southeast, while the main low-latitude current system has moved northwest and is now mainly along the Venezuelan coast.

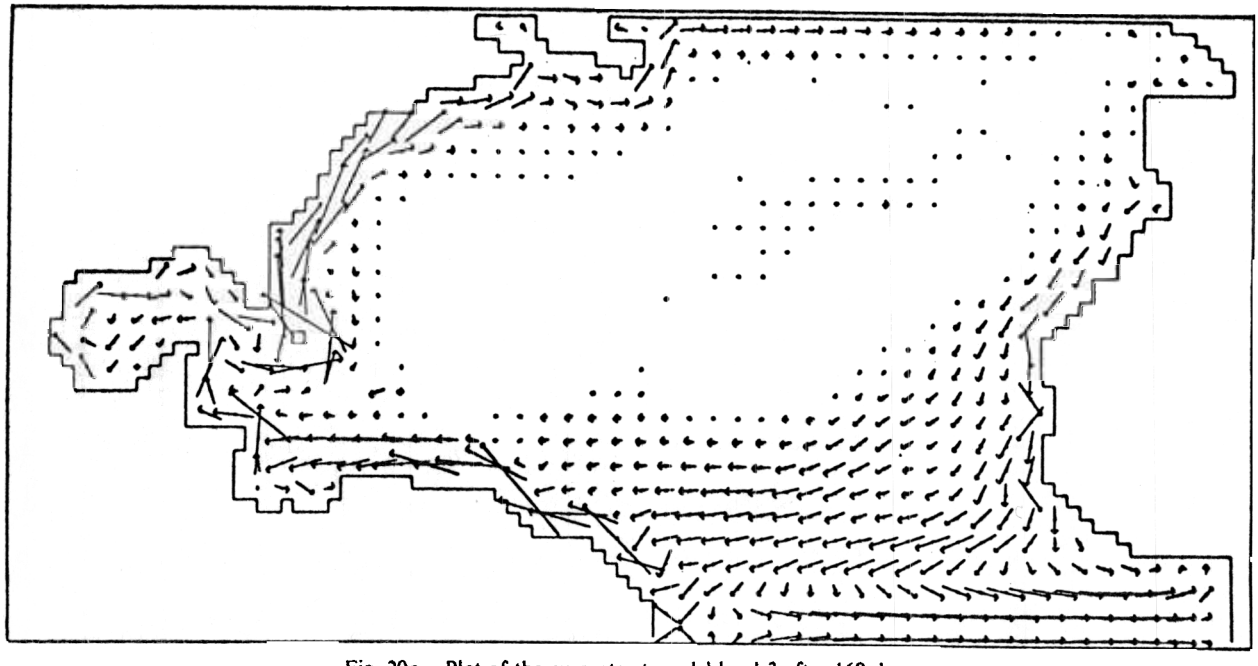

Fig. 20*a*. Plot of the currents at model level 3 after 160 days.

topography is to modulate the response locally. To the east of the mid-Atlantic ridge north of 40°N there is a marked difference, however, which is not qualitative. The flow in Figure 21*a* is southward; in Figure 21*b* it is weakly northward.

Finally, to illustrate the role of the baroclinic field in the western boundary current, a vertical section along 30°N is shown in Figures 22*a* and 22*b* for experiments 3 and 4, respectively. The baroclinic nature of the stream can be seen as well as the way in which stratification allows the Gulf Stream to ride up onto the shelf. In the unstratified case, on the other hand, the stream was at the edge of the abyssal plain. There is no equatorward flow under the Gulf Stream in either case.

Near the equator the high modes become more important. Thus in the Guiana current a more complicated vertical structure prevails. The relative importance of the various modes can be illustrated by plotting the percent variance accounted for by the modes. In Figure 23 we plot the percent variance accounted for by the barotropic and first baroclinic modes after 160 and 1600 days for the zonal velocity. At 160 days the barotropic response is still dominant over most of the basin because of the slow response of the zonal baroclinic modes. This is not true toward the equatorial region, however, as Figure 23*b* shows. Equatorward and south of the first mode the second mode is important in a frontal band rather like that

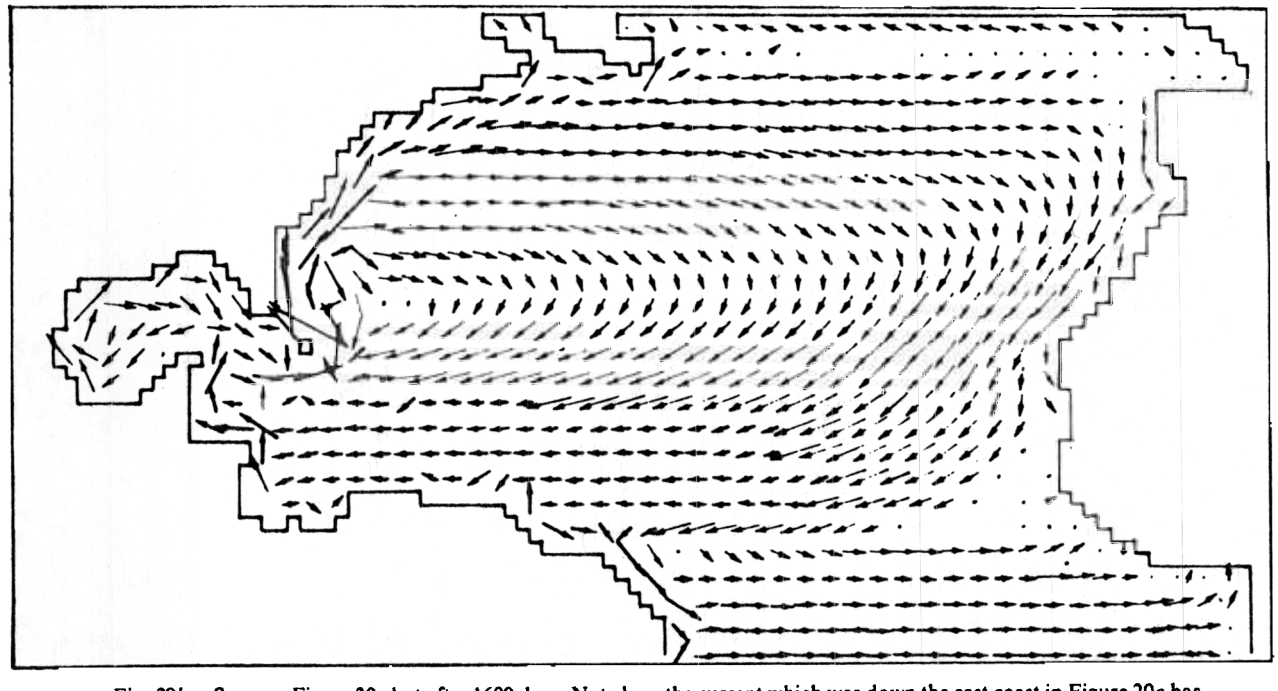

Fig. 20*b*. Same as Figure 20*a* but after 1600 days. Note how the current which was down the east coast in Figure 20*a* has moved offshore associated with the movement of the baroclinic wave fronts in this region. The main change is in the Guiana area, however, where the current has completely reversed and is now feeding the eastward equatorial flow.

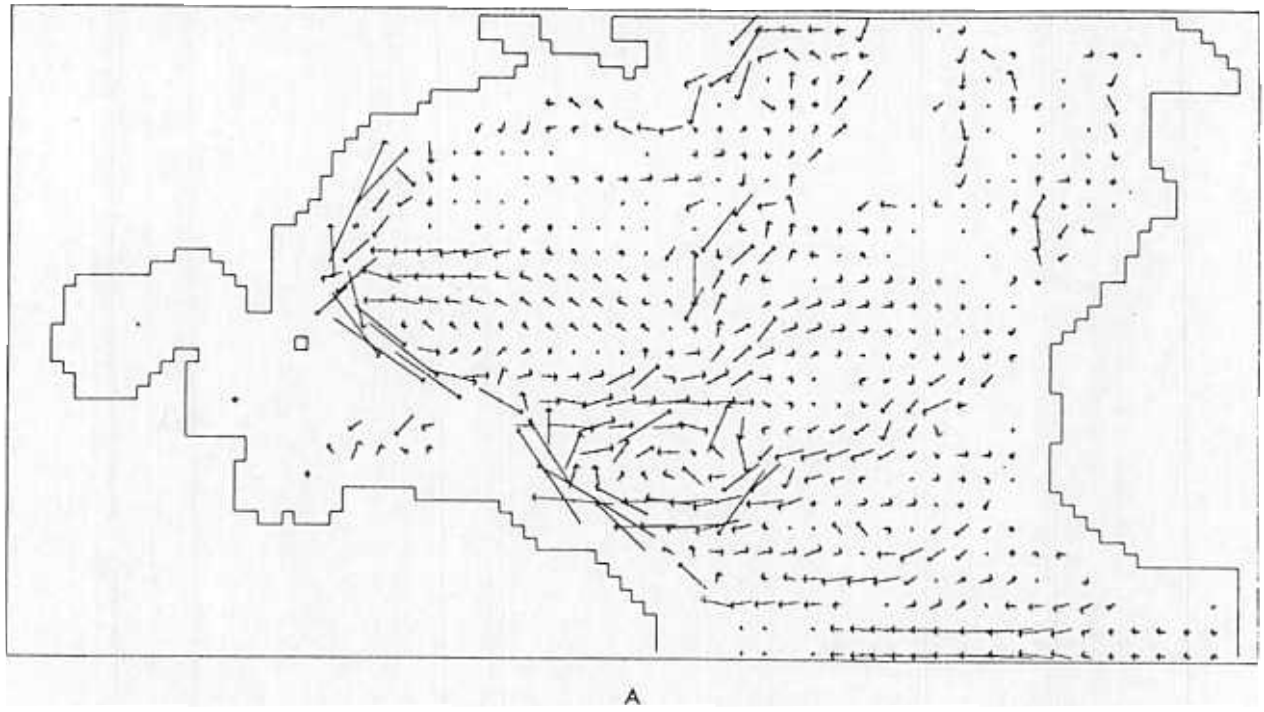

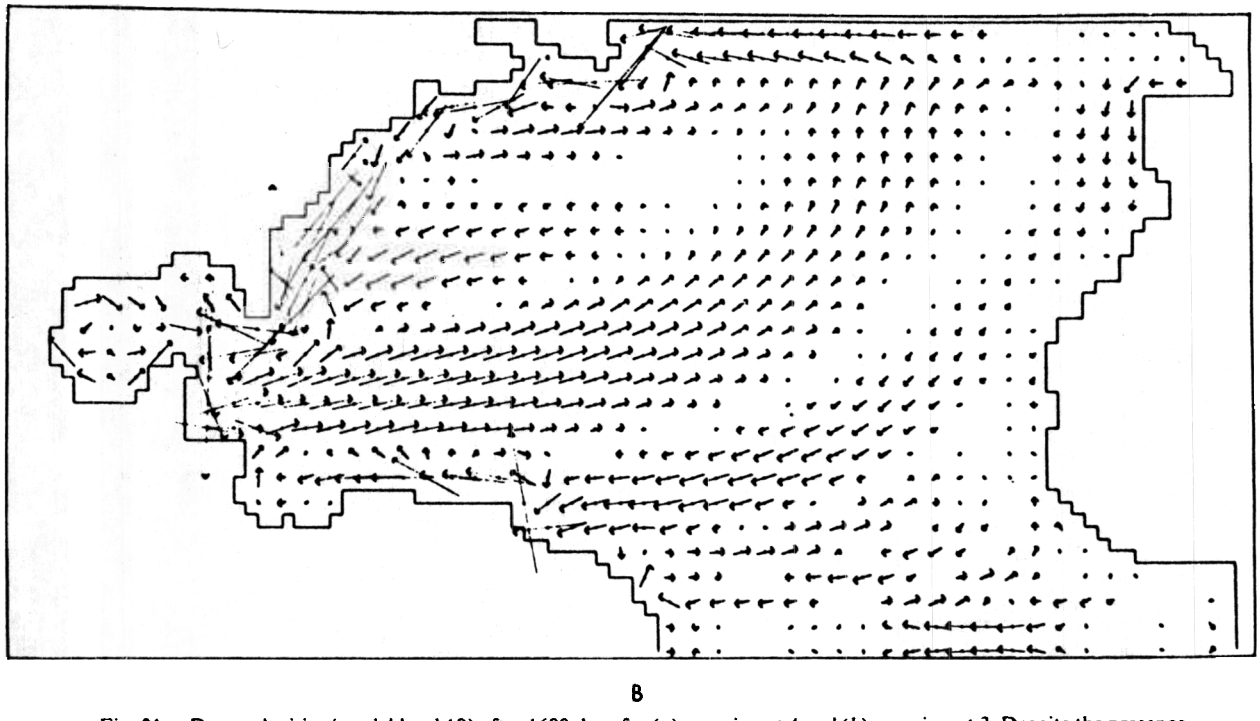

Fig. 21. Deep velocities (model level 10) after 1600 days for (*a*) experiment 4 and (*b*) experiment 3. Despite the presence of topography, the main current systems are the same (associated with baroclinic wave fronts). Comparing Figures 21*a* and 21*b* does show that the topography induces local perturbations in the main current systems, however.

exhibited by the first mode in Figure 23*b*. As time evolves, these 'fronts' move northwestward, and by day 1600 the first baroclinic front has penetrated almost to the Gulf of Mexico (Figure 23*d*). The second mode (not shown) lies to the south, along the Caribbean and stretching up along the Moroccan coast. Higher modes are of some importance at still lower latitudes.

As Figure 23*a* shows, the importance of the barotropic response wanes after its initial importance as the slower baroclinic modes spin up and propagate westward (differentially with latitude).

6. Conclusions

The studies reported here indicate the response characteristics to be expected in the North Atlantic when there is a change of wind forcing and show how important topography, stratification, etc., are in determining those characteristics.

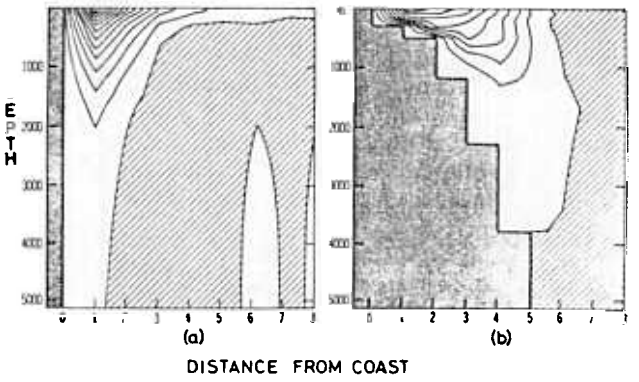

Fig. 22. Vertical section running east-west through the Gulf Stream at 30°N for (*a*) experiment 3 and (*b*) experiment 4 shows how stratification has allowed the current to ride up onto the shelf. In the absence of stratification the transport would be maximum at the foot of the slope (grid point 6). Horizontal numbers indicate grid points from the coast. The contour interval is 2.5 cm/s.

The 100-day simulations exemplify the more rapid response features. These consist of the following:

1. There is a barotropic adjustment within a few days to give a flow approximating the topographically modified Sverdrup interior flow and a western boundary current to close the circulation.

2. Barotropic transients are superimposed upon this flow which are conveniently described in terms of basin modes. These were found to be more prominent over and to the east of the mid-Atlantic ridge than to the west. The gravest mode has a period of 2.6 days and is considerably affected by topography. In the simulation these transients had most of their energy dissipated within 50 days.

3. Upwelling or downwelling occurs around the coasts and along the equator. This is due to the tangential component of the wind and is modified by propagation along the coast or equator.

4. There are inertial period oscillations in the ocean interior. These are modified by propagation, particularly in the meridional direction. Power spectra show peaks at both inertial frequency and a higher frequency.

5. Baroclinic gravity waves propagate into the interior at speed c. In particular, effects propagating in from the northern boundary remove the inertial oscillations.

There are also slower adjustment processes which were studied using 1600-day simulations. This is not sufficient time for a complete equilibrium to be established, but the main adjustments seem to have occurred by this time. The baroclinic adjustment is little affected by bottom topography, so calculations based on a flat-bottomed ocean predict the baroclinic spin-up quite well. However, the interaction of the baroclinic field with bottom topography has an important effect on the barotropic mode. The result is that the barotropic mode has a slow adjustment on the baroclinic time scale. Thus in a few days the barotropic mode becomes established with the flow appropriate for a homogeneous ocean with topography. Over a period of years, however, this changes as the baroclinic mode becomes established and becomes much closer to the flow appropriate to a flat-bottomed ocean.

Other features adjust on this time scale as well. For instance, the 'Gulf Stream' moves up onto the shelf instead of having its maximum at the foot of the continental slope as it does after the rapid adjustment phase.

APPENDIX A

The model used is a linearized version of that described by *Bryan* [1969]. These are no mean currents, and the vertical stratification used in experiments 3 and 4 is independent of horizontal position. The model resolution is 1 degree of latitude and longtitude. In the barotropic runs 1 and 2 the stratification is taken to be zero, whereas in the stratified case we use a mean temperature field given in Table A1. This is related to density by the simplified equation of state

$$\rho = \rho_0 (1 - \alpha T)$$

There are no salinity effects. The equations of motion are

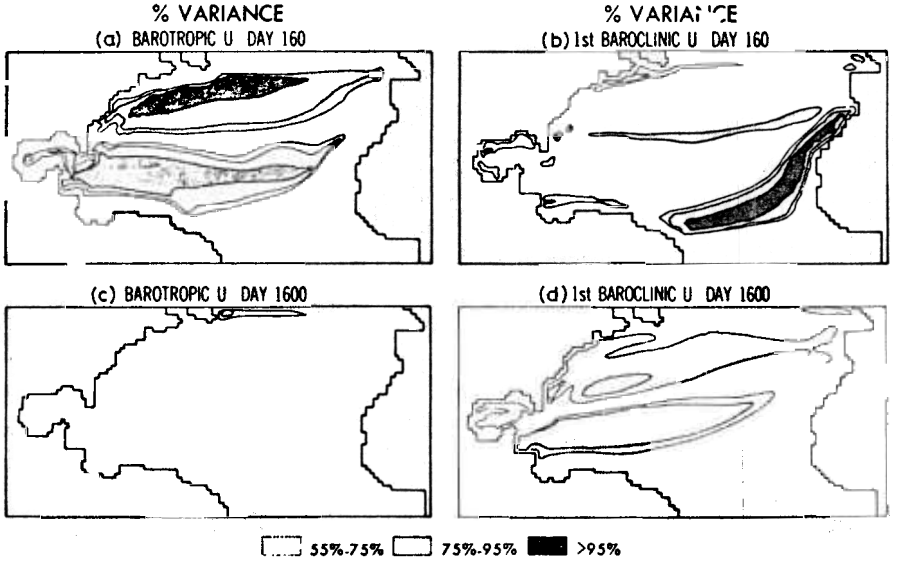

Fig. 23. Percentage variance accounted for by the barotropic and first baroclinic modes for the u-velocity field after 160 and 1600 days. Initially, the response is mainly barotropic in middle latitudes. At lower latitudes and along the eastern boundary there is a strong baroclinic response in the neighborhood of the wave front which propagated westward from the eastern boundary. By day 1600 the middle latitude response is mainly first baroclinic.

TABLE A1. Temperature Structure Used in Experiments 3 and 4

Model Level	Depth of Bottom of Box, m	Depth of Center of Box, m	T, °C
	50	25	20.0000
2	113	82	17.7098
3	205	159	15.1824
4	344	274	13.9960
5	557	451	12.9573
6	870	713	11.6645
7	1305	1087	10.2441
8	1871	1588	9.3877
9	2650	2216	8.9643
10	3350	2955	8.6705
11	4214	3782	8.4328
12	5128	4671	8.2741

$$u_t - fv = -\frac{1}{\rho_0 a \cos\varphi}\frac{\partial p}{\partial \lambda} + K_M\frac{\partial^2 u}{\partial z^2} + A_M\left(\nabla^2 u + \frac{(1-\tan^2\varphi)}{a^2}u - \frac{2\sin\varphi}{a^2\cos^2\varphi}\frac{\partial v}{\partial \lambda}\right)$$

$$v_t + fu = -\frac{1}{\rho_0 a}\frac{\partial p}{\partial \varphi} + K_M\frac{\partial^2 v}{\partial z^2} + A_M\left(\nabla^2 v + \frac{(1-\tan^2\varphi)}{a^2}v + \frac{2\sin\varphi}{a^2\cos^2\varphi}\frac{\partial u}{\partial \lambda}\right)$$

$$\frac{\partial p}{\partial z} = -g\rho$$

$$\frac{1}{\cos\varphi}\frac{\partial u}{\partial \lambda} + \frac{1}{a\cos\varphi}\frac{\partial}{\partial \varphi}(v\cos\varphi) + \frac{\partial w}{\partial z} = 0$$

$$\frac{\partial T}{\partial t} + w\frac{\partial \bar{T}}{\partial z} = K_H\frac{\partial^2 T}{\partial z^2} + A_H\nabla^2 T$$

$$\nabla^2 = \frac{1}{a^2\cos^2\varphi}\frac{\partial^2}{\partial \lambda^2} + \frac{1}{a^2\cos\varphi}\frac{\partial}{\partial \varphi}\left(\cos\varphi\frac{\partial}{\partial \varphi}\right)$$

In none of the experiments was there convective adjustment, but there was vertical and horizontal diffusion of heat and momentum. The value of the horizontal eddy viscosity was $A_M = A_H = 5 \times 10^9$ m²/s. The values of the vertical coefficients K_M and K_H were 100 cm²/s and 5 cm²/s, respectively. It is convenient in the analysis to split the vertical structure into modes. The eigenvalues deduced by this means are given in Table A2.

TABLE A2. Vertical Mode Speeds

Mode	Eigenvalue c, m/s
0	224.00
1	2.71
2	1.38
3	1.00
4	0.77
5	0.63
6	0.56
7	0.48
8	0.45
9	0.38
10	0.35
11	0.33

APPENDIX B

We consider how trapped waves behave as the resolution of the radius of deformation changes. Trapped Kelvin waves can be characterized by (15): $fp_y + p_{xt} = 0$. Consider a wave which is trapped against an eastern coast ($x = 0$) and is propagating northward. The form of the wave is $e^{(f/c)x}e^{i(\omega t - ly)}$. For the exact case this has the dispersion relation

$$\omega/l = c \tag{B1}$$

while in the approximate case it is

$$\frac{\omega}{l} = \frac{2f\Delta}{e^{+\Delta/a} - e^{-\Delta/a}} \tag{B2}$$

where we are considering the north-south propagation errors associated with east-west trapping.

The ratio of numerical to analytical values is

$$\frac{2(\Delta/a)}{e^{\Delta/a} - e^{-\Delta/a}} \tag{B3}$$

For good resolution of the radius of deformation, i.e., a/Δ large, this is $\sim 1 - \frac{1}{6}(\Delta/a)^2$, namely, almost unity but less than unity as Δ/a increases. For poor resolution, i.e., a/Δ small, then (B3) becomes

$$2(\Delta/a)\exp(-\Delta/a)$$

which is $\ll 1$. Thus as the resolution of the radius of deformation decreases, so does the speed of propagation of the coastal wave. This effect was noted in conjunction with Figure 11.

REFERENCES

Anderson, D. L. T., and A. E. Gill, Spin-up of a stratified ocean with applications to upwelling, *Deep Sea Res., 22,* 583–596, 1975.

Anderson, D. L. T., and A. E. Gill, Beta dispersion of inertial waves, *J. Geophys. Res., 84,* 1836–1842, 1979.

Anderson, D. L. T., and P. Killworth, Spin-up of a stratified ocean with topography, *Deep Sea Res., 24,* 709–732, 1977.

Anderson, D. L. T., and P. D. Killworth, Nonlinear propagation of long Rossby waves, submitted to *Deep Sea Res.*, 1979.

Anderson, D. L. T., and P. B. Rowlands, The role of inertia gravity and planetary waves in the response of a tropical ocean to the incidence of an equatorial Kelvin wave on a meridional boundary, *J. Mar. Res., 34,* 295–312, 1976.

Blandford, R., Mixed gravity-Rossby waves in the ocean, *Deep Sea Res., 13,* 941–961, 1966.

Bryan, K., A numerical method for the study of the circulation of the World Ocean, *J. Comput. Phys., 4,* 347–376, 1969.

Cane, M. A., and E. S. Sarachik, Forced baroclinic ocean motions, *J. Mar. Res., 34,* 629–665, 1976.

Charney, J. G., The generation of ocean currents by wind, *J. Mar. Res., 15,* 477–498, 1955.

Csanady, G. T., Motions in a model Great Lake due to a suddenly imposed wind, *J. Geophys. Res., 73,* 6435–6447, 1968.

Gates, W. L., A numerical study of transient Rossby waves in a wind-driven homogeneous ocean, *J. Atmos. Sci., 25,* 3–22, 1968.

Gill, A. E., Models of equatorial currents, in *Numerical Models of Ocean Circulation,* p. 364, National Academy of Sciences, Washington, D. C., 1975.

Gill, A. E., and A. J. Clarke, Wind-induced upwelling coastal currents and sea-level changes, *Deep Sea Res., 21,* 325–345, 1974.

Godfrey, J. S., On ocean spin-down, I, A linear experiment, *J. Phys. Oceanogr., 5,* 399–409, 1974.

Hurlburt, H. E., J. C. Kindle, and J. J. O'Brien, A numerical simulation of the onset of El Niño, *J. Phys. Oceanogr., 6,* 621–631, 1976.

Lighthill, M. J., Dynamic response of the Indian Ocean to the onset of the southwest monsoon, *Phil. Trans. Roy. Soc., Ser. A, 265,* 45–92, 1969.

Longuet-Higgins, M. S., Planetary waves on a rotating sphere, I, *Proc. Roy. Soc., Ser. A, 279,* 446–473, 1964.

Longuet-Higgins, M. S., Planetary waves on a rotating sphere, II, *Proc. Roy. Soc., Ser. A, 284,* 40–68, 1965a.

Longuet-Higgins, M. S., The response of a stratified ocean to stationary or moving wind systems, *Deep Sea Res., 12,* 923-973, 1965*b*.
Matsuno, T., Quasi-geostrophic motions in the equatorial area, *J. Meteorol. Soc. Jap., 44,* 25-43, 1966.
Moore, D. W., Planetary-gravity waves in an equatorial ocean, Ph.D. thesis, Harvard Univ., Cambridge, Mass., 1968.
Moore, D. W., and S. G. H. Philander, Modelling of the tropical oceanic circulation, in *The Sea,* vol. 6, pp. 319-362, John Wiley, New York, 1977.
Pedlosky, J., A study of the time-dependent ocean circulation, *J. Atmos. Sci., 22,* 267-272, 1965*a*.
Pedlosky, J., A note on the western intensification of the oceanic circulation, *J. Mar. Res., 23,* 207-209, 1965*b*.
Philander, S. G. H., The effects of coastal geometry on equatorial waves, *J. Mar. Res., 35,* 509-523, 1977.
Phillips, N. A., Large-scale eddy motion in the western North Atlantic, *J. Geophys. Res., 71,* 3883-3891, 1966.
Platzman, G., Normal modes of the Atlantic and Indian oceans, *J. Phys. Oceanogr., 5,* 201-221, 1975.
Ripa, P., Normal Rossby modes of a closed basin with topography, *J. Geophys. Res., 83,* 1947-1957, 1978.
Sarkisyan, A. S., and V. P. Keondjiyan, Review of numerical ocean circulation models using the observed density field, in *Numerical Models of Ocean Circulation,* pp. 76-93, National Academy of Sciences, Washington, D. C., 1975.
Schulman, E. E., A study of topographic effects, in *Numerical Models of Ocean Circulation,* pp. 147-167, National Academy of Sciences, Washington, D. C., 1975.
Schulman, E. E., and P. P. Niiler, Topographic effects on the wind-driven ocean circulation, *Geophys. Fluid Dyn., 1*(4), 439-462, 1970.
Veronis, G., An analysis of wind-driven ocean circulation with a limited number of Fourier components, *J. Atmos. Sci., 20,* 577-593, 1963.
Veronis, G., Generation of mean ocean circulation by fluctuating winds, *Tellus, 18,* 67-76, 1966.
Veronis, G., Effect of fluctuating winds on ocean circulation, *Deep Sea Res., 17,* 421-434, 1970.
Veronis, G., and H. Stommel, The action of variable wind stresses on a stratified ocean, *J. Mar. Res., 15,* 43-75, 1956.
Wunsch, C., and A. E. Gill, Observations of equatorially trapped waves in Pacific sea level variations, *Deep Sea Res., 23,* 371-390, 1976.
Yoshida, K., A theory of the Cromwell current and of the equatorial upwelling, *J. Oceanogr. Soc. Jap., 15,* 159-170, 1959.

(Received July 18, 1977;
revised July 3, 1978;
accepted July 7, 1978.)